Calhoun
Institutional Archive of the Naval Postgraduate School

Calhoun: The NPS Institutional Archive

DSpace Repository

Theses and Dissertations | 1. Thesis and Dissertation Collection, all items

1955

Radar magnetic modulation using a high frequency inductor alternator power source.

Rodgers, George F.

Massachusetts Institute of Technology

http://hdl.handle.net/10945/14541

Downloaded from NPS Archive: Calhoun

http://www.nps.edu/library

Calhoun is the Naval Postgraduate School's public access digital repository for research materials and institutional publications created by the NPS community. Calhoun is named for Professor of Mathematics Guy K. Calhoun, NPS's first appointed -- and published -- scholarly author.

Dudley Knox Library / Naval Postgraduate School
411 Dyer Road / 1 University Circle
Monterey, California USA 93943

RADAR MAGNETIC MODULATION USING A HIGH FREQUENCY INDUCTION ALTERNATOR POWER SOURCE

George Francis Rodgers

Library
U. S. Naval Postgraduate School
Monterey, California

RADAR MAGNETIC MODULATION USING A HIGH FREQUENCY INDUCTOR ALTERNATOR POWER SOURCE

by

GEORGE FRANCIS RODGERS
B.S., U.S. Coast Guard Academy
(1946)

SUBMITTED IN PARTIAL FULFILLMENT
OF THE REQUIREMENTS FOR THE DEGREE OF
NAVAL ENGINEER
at the

MASSACHUSETTS INSTITUTE OF TECHNOLOGY
May, 1955

ACKNOWLEDGMENT

The author wishes to express his appreciation to Professor David C. White and to Professor J. Francis Reintjes for their very tangible guidance in setting two faltering feet along constructive paths in the course of this work. Additionally acknowledgement is made to the following for assistance along these paths: Boris Subbotin, M. Riaz and Herbert Woodson of the Energy Conversion Group of the Servomechanisms Laboratory and Ed Nalowicz of Lincoln Laboratory, M.I.T.

29782

TABLE OF CONTENTS

	Page
ABSTRACT.	i
ACKNOWLEDGEMENT	ii
TABLE OF CONTENTS	iii
LIST OF ILLUSTRATIONS AND PHOTOGRAPHS	iv
CHAPTER I - INTRODUCTION	
General.	1
Inductor Alternator.	5
Rectangular Hysteresis Materials	14
Modulator Circuitry.	20
CHAPTER II - ANALYSIS AND PROCEDURE	
Inductor Alternator.	25
Design Development of Modulator.	31
CHAPTER III - RESULTS	41
CHAPTER IV - DISCUSSION	59
CHAPTER V - CONCLUSIONS	66
CHAPTER VI - RECOMMENDATIONS.	72
APPENDIX I - RUNGE'S NUMERICAL SOLUTION FOR HARMONICS .	74
APPENDIX II - MODULATOR DESIGN (QUANTITATIVE)	75
BIBLIOGRAPHY.	84

Index de figures

Page

Chapitre I - Introduction 1

Etude de littérature sur l'hydrologie 4

Bassin de Casamance 11

Problématique 14

Chapitre II - Méthodologie

Introduction 17

Description générale du modèle 17

Modèle conceptuel 20

Chapitre III - Validation

Introduction 23

Description des données 23

Calage 24

Validation 25

Chapitre IV - Résultats

Introduction 27

Résultats 27

Chapitre V - Conclusion 34

Bibliographie 36

Annexe A - Programme 37

Annexe B - Données 42

Annexe C - Résultats 44

Annexe D - Graphiques 46

LIST OF ILLUSTRATIONS AND PHOTOGRAPHS

Figure	Title	Page
I	Two Basic Inductor Alternator Types.	4
II	Cutaway View of Alternator	11
III	Square Loop Ferromagnetic Materials.	15
IV	Operating Characteristics of 2J38 Magnetron. .	19
V	Modulator Circuitry.	21
VI	Short Circuit Current & Open Circuit Voltage .	42
VII	Positionally-Variant Inductive Effect of One Phase	44
VIII	Response of One Phase to Field Step.	45
IX	Transient Waveforms.	46
X	Harmonic Content	48
XI	Forms of Inductances	50
XII	Machine Losses	52
XIII	Hysteresis Loop for 538T1	53
XIV	Core Response for 538T1 (Current Drive) . . .	54
XV	System Schematic	56
XVI	Modulator Waveforms.	57
XVII	Experimental Modulator	68
XIX	Inductor Alternator.	69
XX	View of Modulator System	70
XXI	Power Supply	71

Chapter	Title	Page
I	The Early Natural Philosophy Period	1
II	Changing Views of Chemistry	11
III	Modern Trends Revolutionize Industries	21
IV	Chemistry Transformations of Daily Experience	29
V	Analytical Chemistry	43
VI	Some Typical Chemical Plants Visited	49
VII	Partially-Worked Raw Materials Obtained from Mine	54
VIII	Employment of the Trades in Chemical Plants	59
IX	Chemical Industries	64
X	Chemical Research	69
XI	Terms of Employment	80
XII	Routine Duties	92
XIII	Opportunity Open for Girls	99
XIV	Some Employers Use Typical Internal Safety	104
XV	Optics Necessary	114
XVI	Industrial Chemistry	127
XVII	Correspondence Instruction	132
XVIII	Trade Unions	140
XIX	Training of the Chemical Engineer	144
XX	Value of Scholastic Credit	150
XXI	Index	158

CHAPTER I

INTRODUCTION

German Wartime Developments and Present Applicability

It is generally well known that a significant effort of German science was channelled into development and application of magnetic control devices during World War II. The decision to effect this effort was made at a time when there was no particular shortage of vacuum tube components. The motivation behind the move was ascribed to the need for more service reliability. Such reliability would presumably relieve an acute shortage of technical field personnel who were called upon to maintain electronic equipment. Contemporaneously, a similar effort encompassed development of high speed machinery (1).

Credit for the introduction of magnetic devices cannot go to Germany alone, since other countries, including our own, held a greater number of patents employing the magnetic device (2)(3). However, this wartime effort on the part of Nazi Germany is held to be largely responsible for the current renaissance of magnetics.

CHAPTER I

INTRODUCTION

General Description and Detail Specifications

Philosophically, the same premium on technical personnel is with our mechanized society today, where control devices are an ever-increasing and integral part of the progressive automation of our peacetime economy. A rough index as to the extent of our need for technicians can be obtained from contemporary articles in the newspapers wherein the armed forces decry the loss of trained personnel of the technical fields to industry. For example, retention figures on electronic technicians have been the lowest, about 5%.

Today's Problems

One logical solution to the problems posed above, which will apply equally well to both national postures of peace and of emergency, lies in the development of current equipment to the end of achieving a built-in reliability and service ruggedness. This translation of controlled-environment laboratory analyses into production line models is a continuing process today, in which the desirable properties of solid state devices such as magnetic cores, the titanates and the semi-conductors are utilized to improve reliability. Also related to applications of the above named materials, is the move to the use of high speed rotating machinery. Such a move seeks to exploit the backlog of experience and the inherent reliability of the rotating electro-mechanical power modulator, at the same time condensing the volume of space required for a given power demand.

Philosophically, the case for the use of technical personnel is with any mechanized society today, where control devices are an ever-increasing and integral part of the progressive automation of our particular economy. A rough index as to the extent of our need for technicians can be obtained from contemporary articles in the newspapers wherein the armed forces object the loss of trained personnel of the technical fields to industry. For example, retention figures on electronic technicians have been the lowest, about 5%.

Tower's Problem

One logical solution to the problems posed above, which will apply equally well to both technical positions of power and of responsibility, lies in the establishment of courses of education to the end of achieving a built-in reliability and service requirements. This translation of conventional-environment laboratory analyses into production line models is a continuing process today. In which the desirable properties of solid state devices such as magnetic cores, the filaments and the semi-conductors are utilized to improve reliability. Also relates to applications of the above named materials. In the move to the use of high speed rotating machinery. Such a move needs to highlight the dearth of experience and the inherent reliability of the rotating electro-mechanical power modulator, at the same time considering the volume of space required for a given power demand.

Radar Modulation

In this presentation it is desired to investigate a possible reliability improvement as applied to the limited problem of radar modulation. Radar and other pulsed systems are presently an accepted adjunct to sea and air craft. Basic design considerations for these craft emphasize economy of space and operational reliability. Hence, the applicability of more satisfactory solutions is germane. In the course of this investigation, it will be attempted to employ a high speed inductor alternator as the power source for a radar modulator using thin tape magnetic cores as switching devices. The investigation would seek to test the practicability of these in replacement of vacuum tube switching circuitry and power supply, both of which are potential weak links in the system.

Presentation of Investigation

In accordance with the Instructions for Presentation of Theses for the Department of Naval Architecture and Marine Engineering, a description of the inductor alternator and of thin tape cores as applied to this subject is given as introductory material. Similarly a description of the circuitry used is given. General problems of import are discussed as background material. Ensuing chapters deal with more quantitative information developed in the course of the investigation.

FIG. I
TWO BASIC INDUCTOR ALTERNATOR TYPES

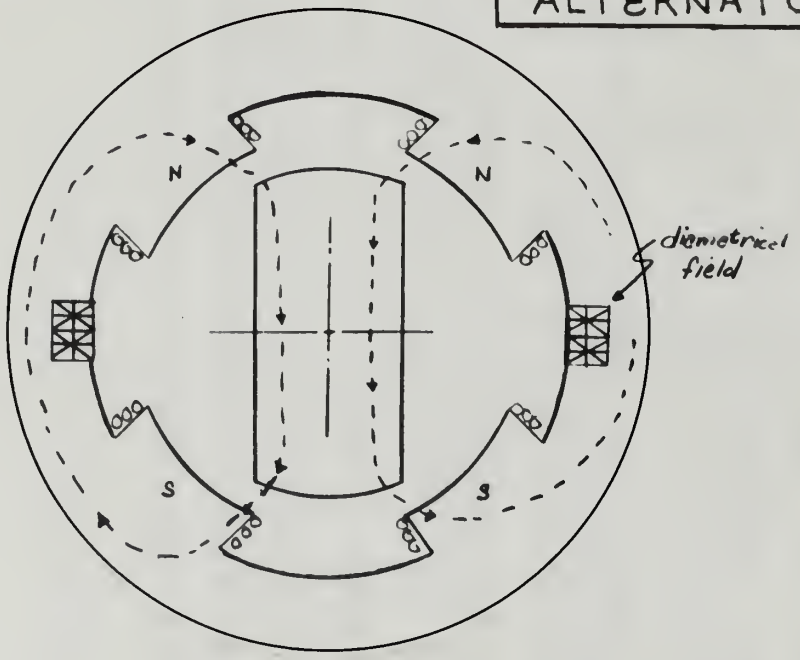

Heteropolar Machine (b)

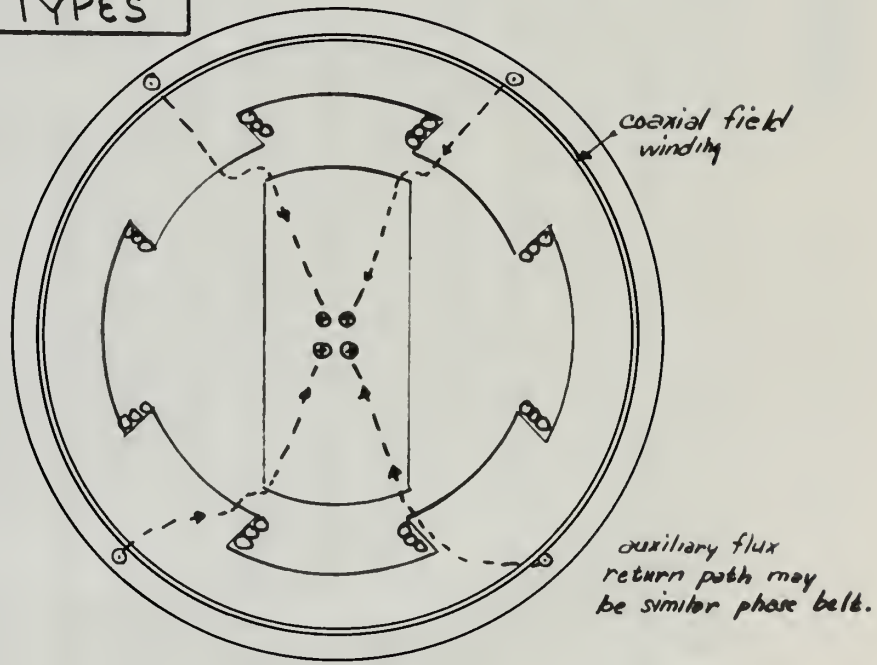

Homopolar Machine (a)

Inductor Alternators

There are two basic types of inductor alternators, homopolar and heteropolar. In the former the excitation field flux crosses the air gap in only one direction; there is a coaxial field coil and there is no flux reversal in the rotor, only a flux pulsation unidirectionally. An example is sketched in Fig. I(a). In the heteropolar machine, the axis of the field coil is mounted diametrically, requiring a flux reversal in the rotor. Figure I(b) illustrates this type of machine. No windings are found on the rotor of either and hence no commutators or slip rings are necessary. The intent of the design is to create a time variant reluctance for the flux path of each winding, by use of saliency on both stator and rotor. It will be seen that as the rotor turns, the air gap flux is gated through each winding in sequence. The effective alternating flux density in the armature winding thus varies from a maximum, limited by saturation, to a value near zero. Hence, the effective flux density variation is about half that for a conventional machine. At sufficiently high frequencies, the inductor alternator becomes competitive with conventional alternator designs, since a large number of poles may be accommodated on the periphery of the air gap, and also because no electrical connections are required on the rotor. It can be seen that the frequency of the output follows the conventional formula:

There are two basic types of inductor alternator, homopolar and heteropolar. In the former the excitation field flux crosses the air gap in only one direction; there is a central field coil and there is no flux reversal in the rotor, only a flux pulsation unidirectionally. An example is sketched in Fig. 1(a). In the heteropolar machine, the axis of the field coil is mounted diametrically, requiring a flux reversal in the rotor. Figure 1(b) illustrates this type of machine. No windings are found on the rotor at either end hence no commutators or slip rings are necessary. The intent of the design is to create a time variant reluctance for the flux path by rotor motion, by use of saliency on both stator and rotor. It will be seen that as the rotor turns, the air gap flux is gated through each winding in sequence. The effective alternating flux density in the armature winding thus varies from a maximum, limited by saturation, to a value near zero. Hence, the effective flux density variation is about half that for a conventional machine. At particularly high frequencies, the inductor alternator becomes competitive with conventional alternator designs, since a large number of poles may be accommodated on the periphery of the air gap, and also because no electrical connections are required on the rotor. It can be seen that the frequency of the output follows the fundamental formula:

$$f = \frac{RPM\ p}{60\ 2} \qquad (1)$$

f = frequency in cycles per second

RPM = rotational speed

p = number of poles on armature

Limitations

An examination of some of the salient limitations is relevant to the study of this machine. A few of these are:

(1) Bearing considerations common to high speed machinery.

(2) Bearing considerations peculiar to machinery mounted on a moving platform.

(3) Bearing considerations peculiar to the inductor alternator.

(4) Mechanical strength of the rotor material.

The power dissipated by a bearing is given without derivation, by Petroff's equation (4):

$$P = \frac{4\pi^2 r^3 L w^2 \mu}{c} \qquad (2)$$

where: P = power loss, hp

μ = viscosity of lubricant (reyns)

$$\eta = \frac{\text{shear stress}}{\text{velocity gradient}} \qquad (1)$$

η = viscosity of Newtonian liquid

Bingham : "plastic flow" is given by

$$f = F - G\eta \qquad (2)$$

Explanation

In consideration of flow of the Newtonian fluid is obtained at low rate of high velocity. It may be flows more

(2) Usually sedimentation occurs at high speed condition.

(3) Usually sedimentation occurs is the laminar flow.

(4) Sedimentation velocity is the Newtonian fluid is a moving platform.

(5) Sedimentation velocity is the Newtonian viscosity.

(6) Sedimentation velocity of the rate material.

The above explained by a formula is given stokes equation is viscosity equation (1)):

$$\eta = \frac{F - G\eta}{v} \qquad (3)$$

r = journal radius, in.
L = bearing length, in.
N = journal speed, rpm
c = radial clearance, in.
K = constant

From this expression it is seen that the heat generated in a bearing is proportional to the square of the speed. Two means can be employed to lower this loss, namely use of a lubricant with a low viscosity and increase of radial clearance. Since high speed bearings generally cannot accommodate deflections as well as other bearings, the extent to which the product r^3L may be manipulated is limited. Air is successfully used as a high speed lubricant; the approximate ratio of its viscosity to that of a light oil is 1666. Air bearings have a low radial load capacity.

This machine uses a ball bearing oil mist system, sinceits designed speed (22,000 rpm) is not too high.

Bearing problems peculiar to mounting on a moving platform involve the gyroscopic moment. For a constant angular velocity, Ω, about an axis perpendicular to the axis of rotation, this moment is given by the formula (6):

$$C = \frac{J \Omega \omega}{g}$$

$$= \frac{Wk^2 \Omega \omega}{g} \qquad (3)$$

$$= \frac{W r_S c \omega}{g} \qquad (3)$$

$$Q = \frac{1}{2} \frac{Q c \omega}{g}$$

where

W = load, lb.
r_S = journal radius, in.
c = bearing length, in.
N = journal speed, rps
c = radial clearance, in.
K = constant

From this expression it is seen that the heat generated in a bearing is proportional to the square of the speed. Two means can be employed to lower this loss, namely use of a lubricant with a low viscosity and increase of radial clearance. Since high speed bearings generally cannot accommodate deflections as well as other bearings, the extent to which the product $r_S^3 c$ may be manipulated is limited. Air is successfully used as a high speed lubricant; the approximate ratio of its viscosity to that of a light oil is 1000. Air bearings have a low radial load capacity.

This machine uses a ball bearing oil mist system, since its designed speed (22,000 rpm) is not too high.

Bearing problems peculiar to mounting on a moving platform involve the gyroscopic moment. For a constant angular velocity, ω, about an axis perpendicular to the axis of rotation, this moment is given by the formula (6):

Where: C = gyroscopic couple, in. lb.

J = moment of inertia of rotor, lb. in.^{2}

ω = angular velocity of rotor, rad./sec.

Ω = an arbitrary constant angular velocity

W = weight of rotor, lb.

k = radius of gyration

It can be seen that the bearing would be designed for a radial load proportional to the weight of the rotor for stationary mounting, each bearing would support a load as follows:

$$L_r = K \frac{W}{2} \qquad (4)$$

Where: W = weight of rotor, lb.

K = constant of design (1.5-4)

The total load on the bearing when used on a moving base such as a ship or aircraft is equal to the usual stationary load plus the gyroscopic moment load, which is time variant. Combining equations (3) and (4) to get the total loading:

$$L_t = \sqrt{\left(\frac{K}{2} + \frac{k^2 \Omega \omega}{g}\right)^2} \qquad (5)$$

Now picking a value for ship's roll which might be realistic for a destroyer type, and assuming that the ship's motion may be approximated by a sine wave:

$$\theta(t) = \theta_{max} \cos \frac{2\pi t}{T}$$

$$\dot{\theta}(t) = \theta_{max} \left(\frac{-2\pi}{T}\right) \sin \frac{2t}{T}$$

$$T = 6 \text{ sec.} \qquad (6)$$

$$\theta_{max} = \tfrac{1}{2} \text{ rad.}$$

$$\dot{\theta}_{max} = \tfrac{1}{2} \frac{2\pi}{6}$$

The maximum bearing load now becomes:

$$L_t = W \left(\frac{K}{2} + \frac{k^2 \Omega \omega}{386 \times 6} \right)$$

$$= W \left(\frac{K}{2} + k^2 \omega \times 1.35 \times 10^{-3}\right)$$

Thus the second term in the brackets does not approach the first term until $k^2\omega$ becomes large, or until large moments of intertia are dealt with or until large rotational speeds are encountered. This explains, of course, why auxiliary diesels which are high speed, are not mounted athwartships. It bears on this problem at hand in that high

$$\theta(t) = -\frac{\omega_0}{2}\sin\frac{\omega_0}{2}t$$

$$\dot{\theta}(t) = -\frac{\omega_0}{2}\left(\frac{\omega_0}{2}t\right)\sin\frac{\omega_0}{2}t$$

$$\omega_0 = 1 \text{ rad/sec}$$

$$\omega_0 = 1 \text{ rad/sec}$$

$$\frac{\omega_0}{2} = \frac{1}{2} \text{ rad/sec}$$

speeds are used with a bearing which is sensitive to radial loading.

A final bearing consideration peculiar to the high speed alternator is that d.c. leakage flux finds a path across the bearing clearance. The combination of this constant flux and the rotating journal forms a minuscle alternator in which high local currents can cause pitting and accelerated wear of the bearing journal. The remedy for this condition has been to increase the reluctance of the bearing air gap.

The mechanical strength of the rotor material itself imposes a limitation. If we assume that disk theory holds (7) we may write down the formula for the stress distribution in the moving rotor as follows:

$$\sigma_r = \frac{3+\mu}{8} \rho \omega^2 (r_o^2 - r^2) \qquad (7)$$

$$\sigma_t = \frac{3+\mu}{8} \rho \omega^2 (r_o^2 - \frac{1+3\mu}{3+\mu} r^2) \qquad (8)$$

In which: σ_r = stress in radial direction, psi

σ_t = stress in tangential direction, psi

r = radius of interest, in.

r_o = outer radius, in.

μ = Poisson's ratio, .3 for steel

ρ = .28/386, unit mass density for steel

ω = rotational speed for rotor, rad./sec.

[illegible] are used with a bearing which is negligible in parallel flanging.

A final bearing consideration peculiar to the high speed flywheel is that d.c. leakage flux finds a path across the bearing clearance. The combination of this counter flux and the rotating journal forms a minuscule alternator in which high local currents can cause pitting and metallurgical wear of the bearing journal. The remedy for this condition lies both to increase the reluctance of the bearing air gap.

The mechanical strength of the rotor material itself imposes a limitation. If we assume that disk theory holds (7) we may write down the formula for the stress distribution in the moving rotor as follows:

$$\sigma_r = \frac{3+\mu}{8}\,\rho\,\omega^2\,(r_o^2 - r^2) \qquad (3)$$

$$\sigma_t = \frac{3+\mu}{8}\,\rho\,\omega^2\,(r_o^2 - \frac{1+3\mu}{3+\mu}\,r^2) \qquad (4)$$

In which σ_r = stress in radial direction, psi

σ_t = stress in tangential direction, psi

r = radius of increment, in.

r_o = outer radius, in.

μ = Poisson's ratio, .3 for steel

ρ = .283/386, unit mass density for steel

ω = rotational speed for rotor, rad./sec.

(10)

FIG. II
CUTAWAY VIEW OF ALTERNATOR

5/13/55 Scale: 1/4" : 1" .54" C.F.E.

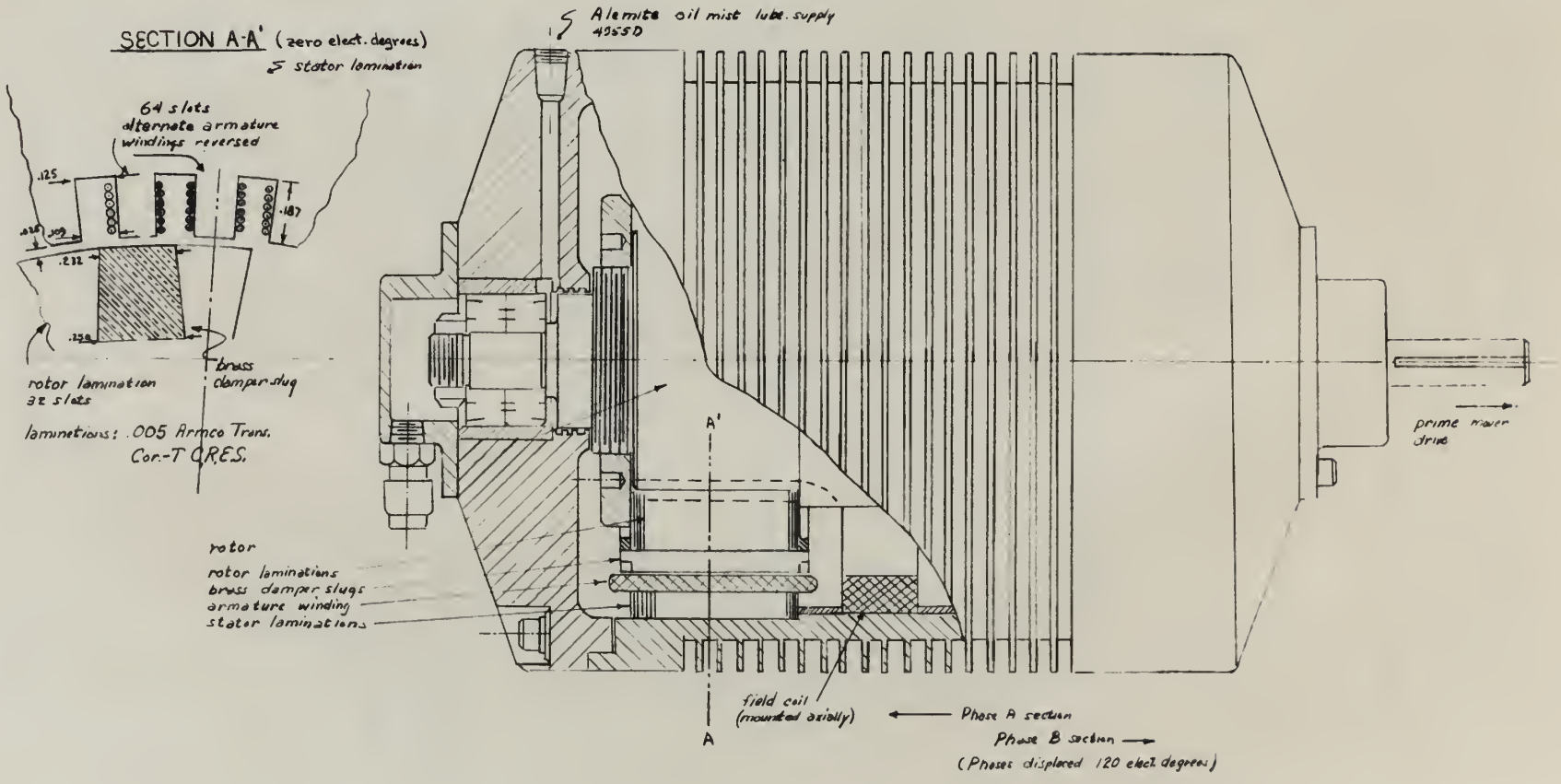

The two stresses are greatest where the radius is zero, or at the center of the rotor, if we assume that the rotor is made up of a single homogenous material. For steel, these stresses become:

$$\sigma_r = \sigma_t = \frac{3+.3}{8} \times \frac{.28}{386} V_o^2 = 3V_o^2 \times 10^{-4} \qquad (9)$$

where V_o is the peripheral speed, in./sec.

For the alternator used in this presentation, which was run at a low speed, 9370 rpm, because of prime mover limitations, we have for the stress at the center of the rotor:

$$\sigma_r = 3 \times 10^{-4} \times \left(\frac{9370}{60} 2\pi \times \frac{4.58}{2}\right)^2$$

$$= 1502 \text{ psi (not accounting for fillet and corner effects)}$$

Conversely, allowing a maximum stress of 25,000 psi, the peripheral velocity is set at 9,150 in./sec. and the speed at 38,300 rpm.

Physical Description of Alternator

The machine used here is a 400 watt homopolar inductor alternator designed to run at 22,000 rpm. A cutaway

view of the machine is shown in Fig. II. High frequency machines, more common in the early days of radio engineering, are applicable industrially today in induction heat treatment.

There are 64 stator teeth and 32 rotor teeth. Brass rotor slugs are mounted between the rotor teeth, the purpose of these being to improve the waveform by shorting out higher frequencies than the fundamental. The field coil is mounted coaxially and the flux path is seen to follow axially along the frame, radially across the air gap, axially back through the rotor, again radially across the second air gap and again axially to the field coil. The two rotor-stator sections are offset such that the denticulated geometry is complementary; thus the net air gap seen by the field flux is a constant. Each stator tooth is wound with 14 turns of #26 AWG magnet wire; alternate stator teeth are oppositely wound. The field coil consists of 574 turns of the same wire. Lubrication is supplied through an Alemite Oil-Mist automatic lubrication system, model 4955D. The frame of the alternator is mounted on a 1 inch steel bed plate. The alternator shaft connects through a spindle to a belt drive, which in turn is driven by a ½ horsepower Dumore Universal Motor, Mod. 5-021.

Rectangular Hysteresis Loop Materials:

For switching circuits in the present state of the art, these materials may be separated into two categories, the ferromagnetic tape cores and the ceramics. The differences in properties of these may be illustrated in Table I, in which an example of each is given:

TABLE I

COMPARISON OF FERROMAGNETIC AND CERAMIC CORE PROPERTIES

	Resistivity	Residual Ind.	D.C. Coercivity	Curie Temp.
	ohm-cm	gauss	oersteds	^{o}C
4-79 Permalloy (ferromagnetic)	5×10^{-5}	8700	.1	1100
MF-1118 Ferramic (ceramic)	10^{7}	1800	1.5	200

It can be seen that the metallic tapes have generally low resistance, high residual inductance and Curie temperature. The ceramics have opposite characteristics but have excellent high speed memory applications since due to high resistance, eddy currents cannot build up. Switching times for the two samples chosen above are 10 and 1 microseconds respectively for a step current drive of twice the coercivity (8).

Ferromagnetic Substances Less Ferrimagnetic

For existing circuits in the present state of the art, these materials may be separated into two categories, the ferromagnetic type cores and the ceramics. The difference in properties of these may be illustrated in Table I, in which an example of each is given:

TABLE I

COMPARISON OF FERROMAGNETIC AND CERAMIC CORE MATERIALS

	Magnetization Coefficient	D.C. Coercivity	Cycle Time
	ohm-cm	Gauss	oersteds	T_0
4-79 Permalloy (Ferromagnetic)	2×10^{-5}	6700	.1	1100
78-III Ferramic (ceramic)	10^{7}	1300	1.5	500

It can be seen that the metallic ferrous core generally low resistance, high retained induction and cycle temperature. The ceramics have commonly observed-ferrites two have excellent high speed memory applications since due to high resistance, only capacity reactor valid as. Switching times for the two samples chosen above are 10 and 1 microsecond respectively for a step overdrive drive of twice the coercivity (0).

FIG III
SQUARE LOOP MATERIALS

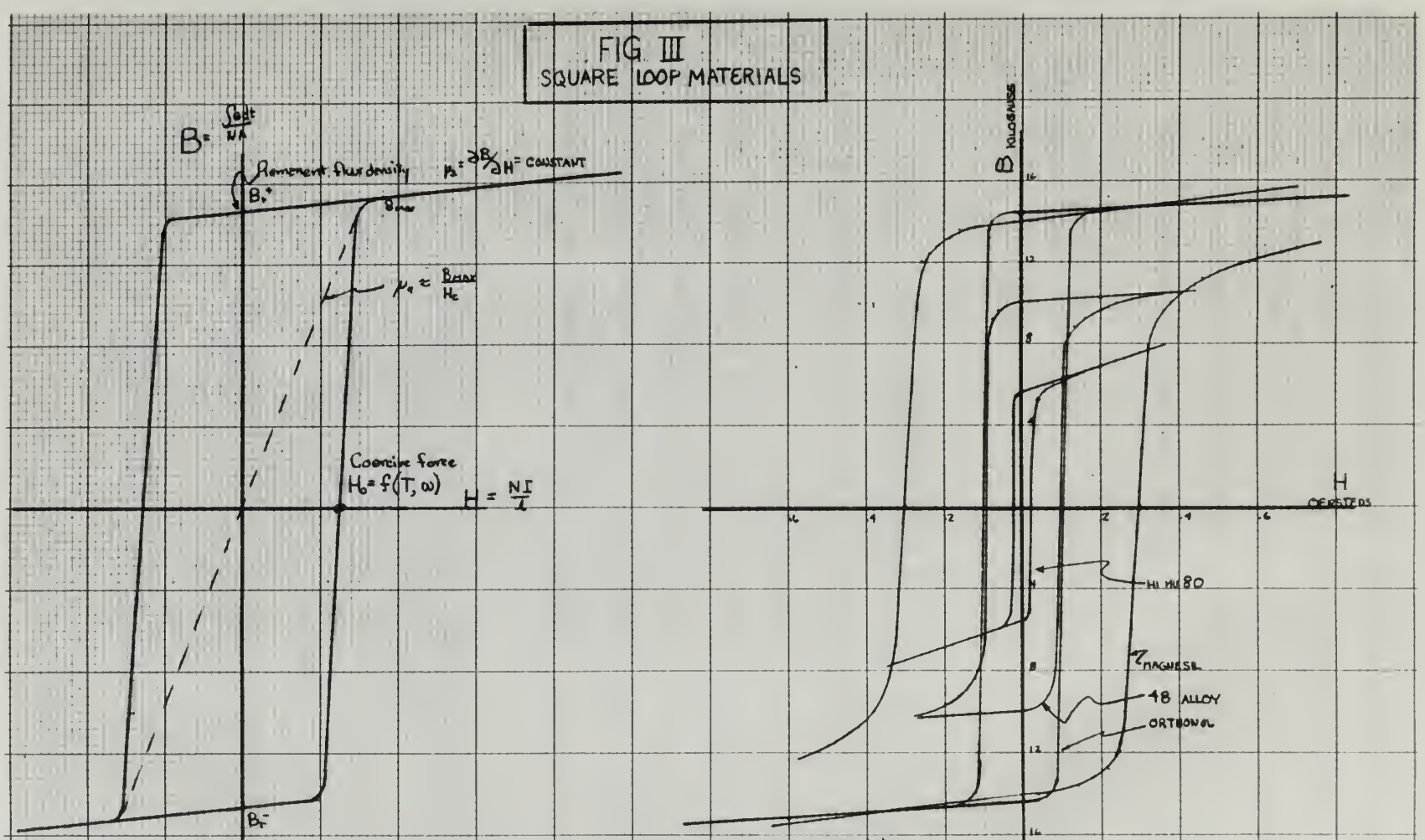

(a)
TYPICAL HYSTERESIS FORM
FOR "SQARE LOOP" MATERIAL

(b)
D.C. HYSTERESIS LOOPS
OF FOUR FERROMAGNETIC MATERIALS
(FROM MAGNETICS, INC. "TAPE WOUND CORES")

The ceramic cores, however, with a high volume to area ratio for mechanical strength and low thermal conductivity are not able to dissipate heat rapidly. The low Curie temperature in conjunction with this last named property causes changes in characteristics at high switching rates. To reduce eddy current effects, the tapes are reduced in thickness to sizes of the order of one mil. The B-H Characteristics of some of the commonly used materials are given in Fig. III.

Cores may be switched with flux drive (voltage) or with current drive, from one remanent state to the other. Generally the current drive is associated with a higher coercive force. This value of coercive force increases with increase in the frequency of switching as a result of higher eddy currents and hence losses. The d.c. hysteresis loop corresponds to the minimum energy required for core switching.

In this application, we are concerned with flux switching of the wound core. Lenz' Law in an integrated form applies:

$$e = -N \frac{d\Phi}{dt} \times 10^{-8} \qquad (10)$$

$$= -NA \frac{dB}{dt} \times 10^{-8}$$

The ceramic cores, however, with a high volume to area ratio for mechanical strength and low thermal conductivity are not able to dissipate heat rapidly. The low Curie temperature in conjunction with this last named property causes changes in characteristics at high switching rates. To reduce eddy current effects, the cores are reduced in thickness to sizes of the order of one mil. The B-H characteristics of some of the commonly used materials are given in Fig. 111.

Cores may be switched with flux delta (voltage) or with current delta, from one remanent state to the other. Generally the current delta is associated with a higher coercive force. This value of coercive force increases with increase in the frequency of switching as a result of higher eddy currents and hence losses. The d.c. hysteresis loop corresponds to the minimum energy required for core switching.

In this application, we are concerned with an integrated form application of the second core. Lenz's law in time evaluating of the second core.

$$\phi = -N \frac{d\phi}{dt} \times 10^{-8} \qquad (32)$$

$$= -N \frac{dB}{dt} \times 10^{-8}$$

Integrating from t = 0 to t_1 at which time the core has changed state from one residual stable state to saturation, we have:

$$\int_0^{t_1} e\,dt = NA\left[(B_r-) - (-B_r^+)\right] \qquad (11)$$

$$\approx 2NA\,B_{max}$$

When the core is driven into the saturated state, it acquires a constant permeability which is very small. This leads to a value of inductance of the winding of the saturated core:

$$L_s \Delta i = N\Delta\Phi \qquad (12)$$

$$= N\left[\mu \frac{N\,\Delta i}{l}\right] A$$

$$L_s = \frac{3.2\,\mu_s\,N^2 A}{l_m} \times 10^{-8} \qquad (13)$$

Where: $\mu_s = \frac{\partial B_s}{\partial H}$, a constant

A = area of core, square in.

N = number of turns

l_m = meany length of "toroid", in.

$$= \left[\frac{\pi}{2} \right]$$

$$= \frac{\pi}{2}$$

Similarity to Switch Operations

There is no single value of μ which is applicable to the core in the transition state from one remanent state to the other. However, if we look at the locus of operation, i.e. the hysteresis loop, we see that for a tall slender loop a value may be assumed equal to B_m/H_c as shown in Fig. III (a). This permits an approximation to the time variant inductance of the wound core in switching. Thereby, we have an approximate gauge as to the effectiveness of the switch in the ratio μ_u/μ_s or $B_m/\mu_s H_c$. This is because this ratio is the equivalent of the ratio of the "open-switch" inductance to the "closed-switch" inductance in an impedance element made up of inductance alone. Melville (2) gives a figure of 2000 as desirable for this ratio for pulse circuit application.

Associated with the material of the core is a maximum flux density variation, shown on Fig. III(a) as $B_{max.}$ ($B_{max.} \approx B_r$ for our purposes). Since a large $B_{max.}$ permits fewer turns on the winding for the same voltage-time integral, i.e. the same switching waveform. We would like to use a material which has a large $B_{max.}$, consistent with other criteria. Having a smaller number of turns leads to a smaller saturated inductance.

Similarity to Impact Operations

There is no single value of η which is applicable to the core of the transition zone for a resonant state to the atom. However, if we look at the locus of operations, i.e. the hydrogenic loop, we can find a well founded loop a value may be assigned equal to η_{H}^{0} as shown in Fig. III (a). This permits an approximation to the flow vectors immediately of the second order to subsist. Thereby, we have an approximate guide later as to the effectiveness of the method in the ratio η_{H}/η_{H}^{0} or η_{H}/η_{H}^{0}. This is however this ratio is the equivalent of the ratio of the "open-outlet" resonance to the "closed-outlet" resonance in an independent element made up of radioactive atom. Table (I) gives a figure of 2000 as desirable for this ratio for pulse circuit application.

Associated with the material of the core is a maximum flux density variation, shown as Fig. III(a) as $B_{max.}$ ($B_{max.} \geq B_{r}$ for most purposes). Since a large $B_{max.}$ permits fewer turns on the winding for the same voltage-time integral, i.e. the same switching operations. We would like to use a material either has a large $B_{max.}$, combined with either criteria. Having a smaller number of turns leads to a smaller saturated inductance.

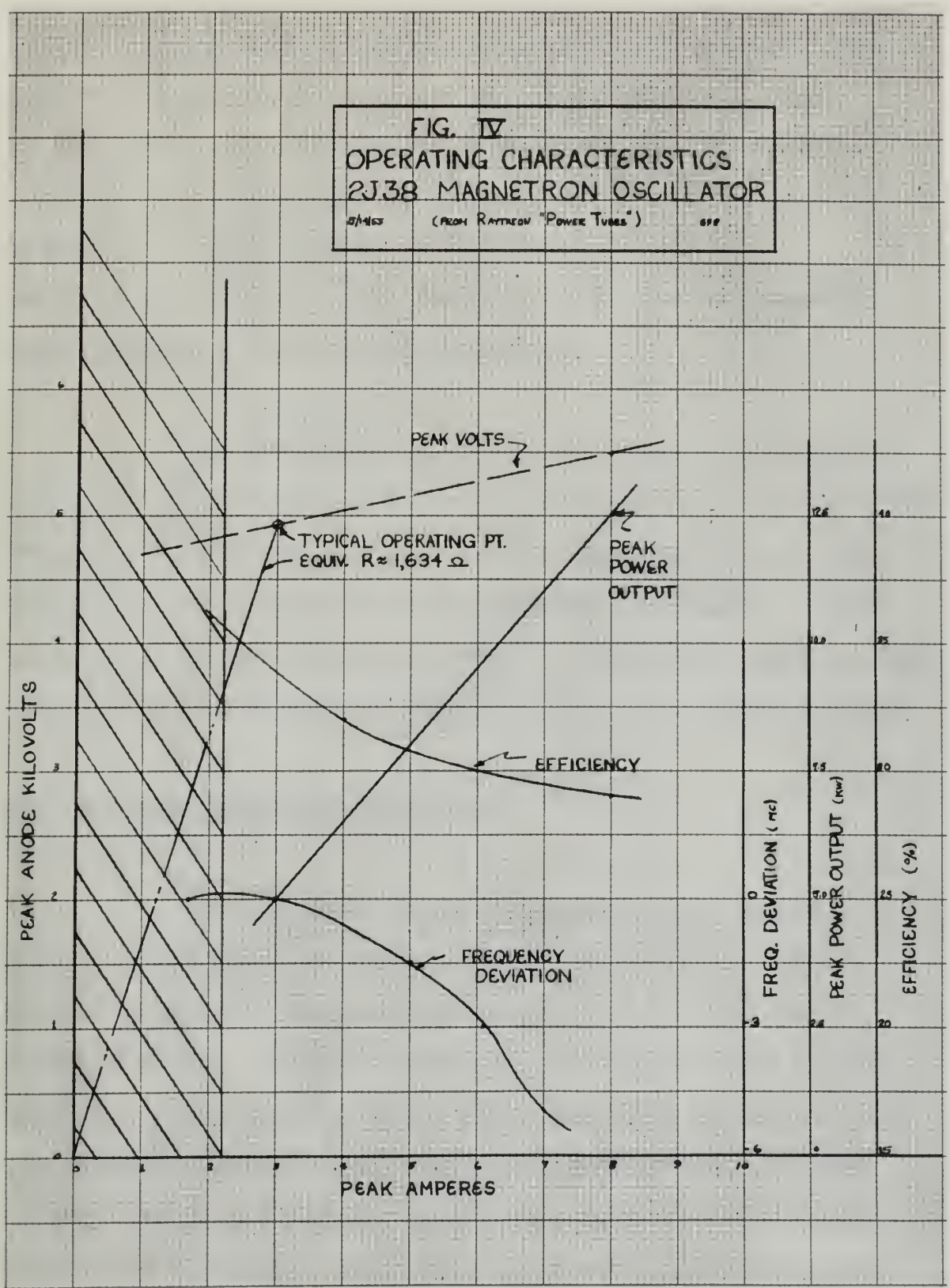
FIG. IV
OPERATING CHARACTERISTICS
2J38 MAGNETRON OSCILLATOR
(FROM RAYTHEON "POWER TUBES")
PEAK VOLTS
TYPICAL OPERATING PT.
EQUIV. R ≈ 1,634 Ω
PEAK POWER OUTPUT
EFFICIENCY
FREQUENCY DEVIATION
PEAK ANODE KILOVOLTS
PEAK AMPERES
FREQ. DEVIATION (MC)
PEAK POWER OUTPUT (KW)
EFFICIENCY (%)

The energy loss, or cost of switching for one cycle is given by the area of the hysteresis loop hence we look for a material with the smallest coercive force. In addition to this, the transition to the saturated state should be a sharp change, as evidenced by the sharp knees of the loop. Note on Fig. III(b) that this transition is less pronounced for certain materials.

The cyclic switch developed here is not exactly analogous to an ordinary switch in the respect that the waveform here determines the time of switching in lieu of this time being established by an independent mechanism. There is another degree of control over the switching point in that the core may be biased externally from a d.c. current source.

Use in Radar Modulator Circuitry

The greatest numbers of operational radars employ a magnetron oscillator in the transmitter. Some typical characteristics are given in Fig. IV, for the Raytheon 2J38. It will be seen in this figure that for a specified plate voltage there is a specified deviation from its operating frequency. Since what goes out of a radar transmitter must return if there is a target, the receiver must be of sufficient band width to accept all echoed out-

FIG. V
MODULATOR CIRCUITRY

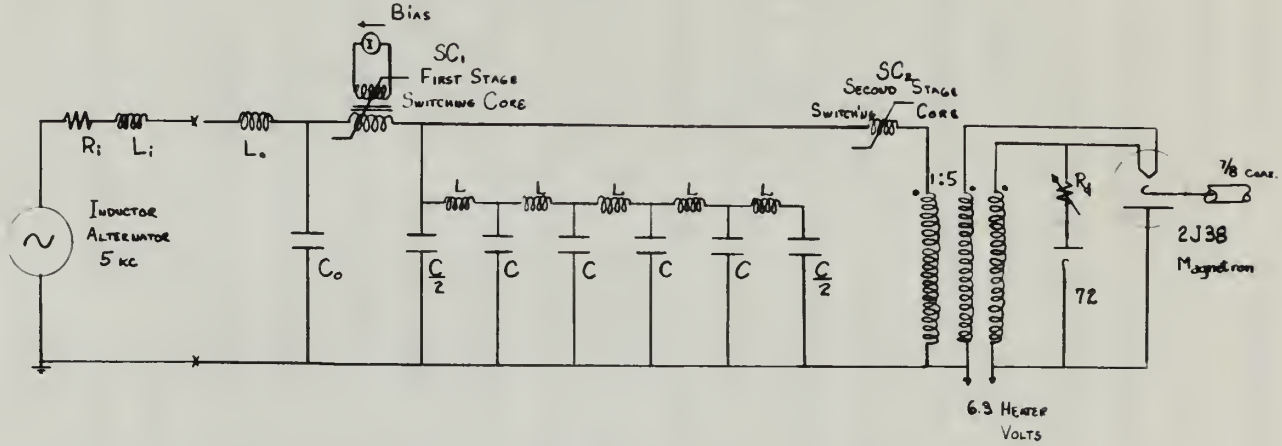

The circuit is best analyzed by 3 piecewise linear circuits which are shown below:

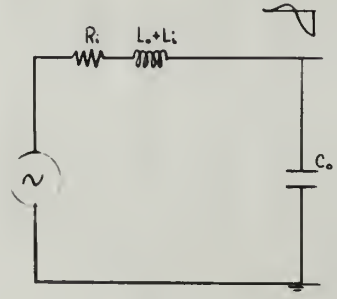

(a)
Charging Circuit
($\approx$ 200 μs)

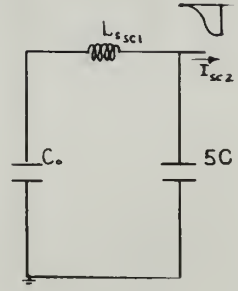

(b)
Intermediate Discharge Circuit
($\approx$ 10 μs)

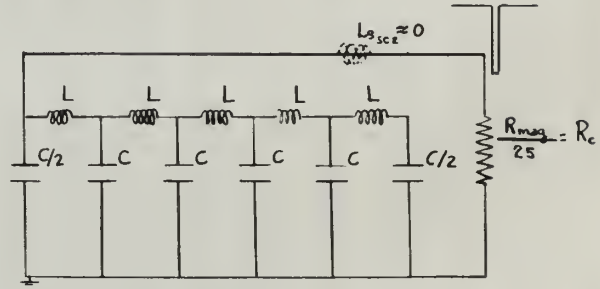

(c)
Final Discharge Circuit
($\approx$ 1 μs)

going frequencies. It follows that the magnetron should be pulsed with a square voltage wave in order to minimize the receiver bandwidth. The bandwidth should be minimized in general, on a search radar at least, in order that the signal/noise ratio is acceptable. A wide frequency drift in transmission, without compensatory circuitry, would reduce the effective range of the equipment. Compensating circuits are costly. Modulator circuitry employs switching devices, cores, hard or gaseous tubes, rotary spark gaps, etc., which are subject to extremely high peak currents and voltages. It is at this point where an improvement on the core device could achieve substantial gains in reliability. Cores have been used in modulation for years, the principle objection to their use in the past has been resultant poor pulse shape. The purpose of this investigation is to determine the advantages devolving from the use of cores in a cascaded circuit for the purpose of improvement of pulse shape. A diagram of the circuit used in this investigation is shown in Fig. V. This circuit was developed and tested for a 250 volt output pulse (10) at a prf of 10 kc. Component values are derived in Appendix II; literal derivation of the proper values for the design is detailed in Chapter II. A qualitative explanation is offerred here preliminarily before more elaborate analysis.

is offered here preliminarily before more elaborate analysis.

detailed in Chapter II. - qualitative explanation

derivation of the pseudo voltage for the design is

components values are derived in Appendix III listed

for a 250 volt output pulse (10% of a 1pf at 10 kc,

shown in Fig. V. This circuit was developed and tested

a diagram of the circuit used in this investigation is

through the purpose of improvement of pulse shape.

advantages derived from the use of cores in a cascaded

The purpose of this investigation is to determine the

used in modulation for years, the potential objection to

their use in the past has been resistance power pulse shape.

could achieve substantial gains in reliability. Cores have been

It is at this point where an improvement to the core device

are subject to extremely high peak currents and voltages.

core, hard or ferrous tubes, rotary spark gaps, etc., which

capacity. Mechanical circuitry employs switching devices,

the effective range of the equipment. Compensating circuits are

in transmission, without compensatory circuitry, would reduce

signal/noise ratio is acceptable. A wide frequency split

to receive, on a second range at least, in order that the

the receiver bandwidth. The bandwidth should be minimized

be pulsed with a square voltage wave in order to eliminate

going frequencies. It follows that the compression should

Description of Operation

The piecewise linear circuit shown in Fig. V (a) is valid over the greatest part of the pulse repetition period. This is a series a.c. resonant circuit whose natural frequency is that of the prf. A voltage transient charges the capacitor C_o up to a value about three times the driving source steady-state peak value. At the first negative peak of the waveform the biased saturable core SC1 switches and the circuit of Fig. V (b) is valid for a period of about 1/20 th of the pulse repetition period. In this time the capacitor C_o dumps its charge into the lumped capacitance of the artificial transmission line which makes up the pulse forming network. This is done in a resonant surge in a time determined by the values of saturated inductance of SC1 and the two equivalent capacitors in series, C_o and 5C. This resonant surge of current causes the PFN to charge to the original peak voltage at C_o at thefirst negative peak. At this time the saturable core, SC2, switches to an effective inductance of zero, causing the charged transmission line to be terminated in its characteristic impedance as viewed across the pulse transformer input. The circuit of Fig. V (c) is valid for this case. The PFN line then delivers a rectangular pulse to the magnetron. The function of the damping diode is to suppress parasitic oscillation caused by stray capacitance at the end of the pulse.

Summary

With the foregoing as preliminary background it is seen that radar modulation is one phase of the field in which reliability improvement might be feasible. Saturable core reactors are used at lower pulse repetition frequencies with some disadvantages, namely poor pulse shape, poor efficiency and the necessity for an alternating source (2) (11). An inductor-alternator, a high frequency electro-mechanical power modulator will serve as the power source for a full-scale modulator network developed previously with success at a 250 volt level and a different pulse repetition frequency (10). It is attempted to obtain a p.r.f. as high as consistent with power limitations on the prime mover.

CHAPTER II

ANALYSIS AND PROCEDURE

Basic Assumptions for Alternator Analysis

Since in its present application the alternator will be working in a repetitive transient mode, it would be mathematically convenient to represent the electrical portion of the machine as groups of inductively coupled circuits. There will, in general, be inductive terms in the grouping which are constants and those which will depend upon rotor position for magnitude. Saturation effects are assumed absent and only first and second harmonic effects are considered.

Vizualization of One Pole-pair

Figure II shows a view of geometrical relationships for one angle of rotor position which may arbitrarily be called zero degrees. If we consider the two end sections

of the stator-rotor assembly as corresponding to two phase belts displaced by 120 electrical degrees, we may say that examination of one pole pair gives full information as to geometrical events occurring with respect to its phase belt. This same pole pair shows events transpiring in the other phase albeit displaced by the phase angle.

Figure II shows the method used in winding the armature. Note that each pole is oppositely wound from its neighour. As the rotor moves it can be seen that the flux path for armature flux in a radial plane is identical at 0^{o} and at 180^{o}, having gone through a complete of geometry in this angle. Therefore, it can be expected that the armature phase self inductance will consist of a term as follows:

$$L_{aa} = L_{aa1} + L_{aa2} \cos 2\varphi \qquad (13)$$

L_{aa} = instantaneous armature phase inductance

L_{aa1} = constant component of L_{aa}

L_{aa2} = variant component of L_{aa}

φ = rotor angle in electrical degrees

= 32 x θ (θ = mechanical degrees of rotation)

of the stator-rotor assembly as corresponding to two phase
belts displaced by 120 electrical degrees, we may say that
examination of one pole pair gives full information as to
geometrical events occurring with respect to its phase
belt. This same pole pair shows events occurring in the
other phase belt displaced by the phase angle.

Figure 12 shows the method used in winding
the armature. Note that each pole is physically wound
from its neighbor. By the rotor curve it can be seen
that the flux path for armature flux in a radial plane is
identical at 0^0 and at 180^0, leaving zone through a complete
of geometry in this angle. Therefore, it can be supposed
that the armature phase self inductance will consist of a
term as follows:

$$L_{aa} = L_{aal} + L_{aa_2} \cos 2\phi \qquad (13)$$

L_{aa} = instantaneous armature phase inductance

L_{aal} = constant component of L_{aa}

L_{aa_2} = variant component of L_{aa}

ϕ = rotor angle in electrical degrees

= $\frac{1}{2}\theta$ (θ = mechanical degrees of rotation)

Similarly, for the mutual term between field and each phase, as the rotor traverses a pole pair ($\gamma = 360^{\circ}$), the geometrical relationships go through one complete cycle. The air gap there varies from a minimum at $\gamma = 0^{\circ}$ to a negative minimum at $\gamma = 180^{\circ}$, (where the rotor tooth is opposed to the oppositely wound stator tooth) and on to $\gamma = 360^{\circ}$ which completes the cycle. Thus:

$$L_{fa} = L_{fa1} + L_{fa2} \cos \gamma \qquad (14)$$

L_{fa} = unidirectional mutual coupling from field to armature (phase a)

L_{fa1} = constant component of L_{fa} (phase a)

L_{fa2} = component with positional dependency upon rotor.

(for phase b add 120°)

Tooth and slot relationship are such that the air gap path for the field flux is almost a constant. Thus there is no positional dependency for the field self inductance.

$$L_{ff} = L_f \qquad (15)$$

A rather special case exists for the mutual term from the armature to the field. It may be qualitatively

envisioned that, due to the oppositely wound armature structure, there is no flux component in the axial direction due to armature current. Thus the mutual term is cancelled out due to zero linkage:

$$L_{fa} \neq L_{af}\,;\, L_{ab} = L_{bf} = 0 \qquad (16)$$

To this point, the brass damper slugs located between rotor teeth have been happily ignored (see Fig. II). The function of these bars is to improve the wave form by shorting out higher frequency components. For a steady state mode of operation for the alternator, it might be feasible to make a point by point calculation of the net air gap flux by graphical solution of La Place's Equation in the air gap. Local areas of saturation, if any, could be assessed and thereby a quantitative analysis of the air gap field attained. This method might also have value in the transient mode.

The analogy might be made that these damper slugs are similar to amortisseur windings, which windings are ignored in some analyses of synchronous machines. Here, however, the slugs occupy a considerable sector of air gap periphery.

Replacement of the damper slug by a fictitious winding is a possibility. No unique current path is present, of course.

The ensuing presentation will ignore the presence of these damper slugs for the time being and will check these effects in data evaluation.

Equations of Alternator

With the foregoing assumptions the forms of inductances have been defined. It is now feasible to write down the electrical equations for the machine as visualized

$$e_f = i_f R_f + \frac{d}{dt}(i_f L_f) \tag{17}$$

$$e_a = \frac{d}{dt}(i_f)\left[(L_{fa1} + L_{fa2}\cos\varphi)\right] - i_a R_a - \frac{d}{dt}(i_a)\left[(L_{aa1} + L_{aa2}\cos 2\varphi\right. \tag{18}$$

$$e_b = \frac{d}{dt}(i_f)\left[L_{fb2} + L_{fb2}\cos(\varphi + 120)\right] - i_b R_b - \frac{d}{dt}(i_b)\left[L_{bb1} + L_{bb2}\cos(2\varphi + 240^\circ)\right] \tag{19}$$

Where: e_a and e_b = phase voltages

e_f = field voltage

Since the phase voltages are not to be used directly in application to the modulator, a new voltage is defined below which is the difference of the phase voltages. A like treatment is made for the currents:

$$e_x = e_a - e_b \tag{20}$$

$$i_x = i_a - i_b \tag{21}$$

Also, from symmetry it is assumed:

$$L_{aa} = L_{bb} \quad ; |L_{fa}| = |L_{fb}| \tag{22}$$

Therefore, equations (18) and (19) are combined below. The constant terms of the mutual of field to armature are retained since sign has not been defined:

$$e_x = \frac{d}{dt}(i_f)\left[L_{fa1} + L_{fa2}\cos\varphi) - (L_{fb1} + L_{fb2}\cos(\varphi + 120^\circ)\right] - i_x(2R_a) - \frac{d}{dt} i_x \left[2L_{aa1} + \sqrt{3}L_{aa2}\cos(2\varphi + 30^\circ)\right]$$

$$e_x = \frac{d}{dt}(i_f)\left[L_{fa1} - L_{fb1} + \sqrt{3}L_{fa2}\cos(\varphi - 30^\circ)\right] - i_x 2R_a - \frac{d}{dt} i_x \left[(2L_{aa1} + \sqrt{3}L_{aa2}\cos(2\varphi + 30^\circ)\right] \tag{23}$$

If the simplifying assumption is made that the second harmonic term is of negligible importance, which may be justified later and also using p for the operator $\frac{d}{dt}$:

$$e_x = p(i_f)\left[L_{fa1} - L_{fb1} + \sqrt{3}\, L_{fa2} \cos(\rho - 30^\circ)\right] - i_x\left[2R_a + 2pL_{aa1}\right] \qquad (24)$$

If the field excitation is supplied from a constant current source, alternator behavior may be described as follows if constant speed is assumed, (the phase angle is dropped):

$$e_x = I_f\left[\alpha\sqrt{3}L_{fa2} \sin(\omega t)\right] - i_x\,(2R_a + 2pL_{aa1}) \qquad (25)$$

The procedure to be followed later will be to evaluate the various constants of the machine by conventional methods and to thereby provide a check on the foregoing analysis.

Development of Modulator Circuitry

The next stage in the design of the full scale magnetic modulator is to expand on the operation of the circuitry to be used. As mentioned in the introduction, a low voltage model of this basic circuit was operated

successfully in Reference 10. A review of the mechanics of operation of the circuit is in order for this presentation. For convenience in analysis, there are three piecewise linear approximations to the cyclic operation. These are shown in Fig. V and are in order, the charging circuit, the intermediate discharge circuit and the final discharge circuit.

The Charging Circuit

In the charging portion of the cycle, the alternator causes the voltage on C_o to rise in a conventional, full cycle, a.c. resonant charging mode. (11) The piecewise linear circuit for this mode is valid over the greatest part of the cycle. The inductor L_o is placed in series with the internal inductance of the alternator to bring the series LC combination to the proper magnitude for resonance. It is possible, with no limitations as to choice of other circuit components to match C_o to the internal inductance of the machine. [In the case at hand, the pulse transformer turns ratio was limited to 1:5 which in turn imposed another constant through the pulse forming network.] Note that the circuit is considered to be open to the right of C_o due to the high impedance presented by the first saturable core. Starting with the alternator

voltage in La Place notation; operating on the circuit.

$$I_{(s)} = \frac{e_{(s)}}{z_{(s)}} \tag{24}$$

$$I_{(s)} = \frac{\left[\sqrt{3}\,\frac{\Omega\ L_{fa_2}\ \omega}{s^2+\omega^2}\right]}{\frac{1}{sC_o} + sL_t + R_1}$$

$$E_{co} = \frac{I_{(s)}}{sC_o}$$

$$E_{co} = \frac{1}{sC_o}\ \frac{\left[\frac{\Omega\ \sqrt{3}\ L_{fa_2}\ \frac{\omega}{s^2+\omega^2}}{}\right]}{\left[s^2 + \frac{sR_1}{L_t} + \frac{1}{LC_{to}}\right]\frac{L_t}{s}}$$

$$= \frac{1}{LC_{to}}\,\Omega\sqrt{3}\,L_{fa_2}\left[\left(\frac{\omega}{s^2+\omega^2}\right)\left(\frac{1}{s^2 + \frac{sR_1}{L_t} + \frac{1}{LC_{to}}}\right)\right] \tag{27}$$

Notice the three nontrivial conditions on the elements.

$$\frac{\left[\frac{\omega}{\omega+\omega_1}\right]}{\frac{1}{\omega_1^2}+\frac{1}{\omega^2}+\frac{1}{\omega^2}} = \frac{\left[\frac{\omega}{\omega+\omega_1}\right]}{\frac{1}{\omega_1^2}+\frac{1}{\omega^2}+\frac{1}{\omega^2}}$$

$$\frac{\left[\frac{\omega}{\omega+\omega_1}\right]}{\frac{1}{\omega_1^2}+\frac{1}{\omega^2}+\frac{1}{\omega^2}} = \frac{\left[\frac{\omega}{\omega+\omega_1}\right]}{\frac{1}{\omega_1^2}+\frac{1}{\omega^2}+\frac{1}{\omega^2}}$$

$$= \left[\left(\frac{\omega}{\omega+\omega_1}\right)\left(\frac{\omega}{\omega+\omega_1}\right)\right]$$

$$E_{co} = \left[\frac{R'}{C_o s}\right]\left[\frac{s/L_t}{s^2 + \frac{R_1 s}{L_t} + \frac{1}{L_t C_o}}\right]$$

$$= \frac{I_f \Omega \sqrt{3}\ L_{fa_2}}{L_t C_o}\left[\frac{\omega}{s^2+\omega^2} \times \frac{1}{s^2 + \frac{R_1 s}{L_t} + \frac{1}{L_t C_o}}\right]$$

Letting: $\frac{1}{L_t C_o} = \omega^2$

$$\frac{R}{2L_t} = \alpha$$

$$E_{co} = \frac{I_f \Omega \sqrt{3}\ L_{fa_2}}{L_t C_o}\left[\frac{\omega}{(s^2+\omega^2)(s+\alpha-j\omega)(s+\alpha+j\omega)}\right] \quad (29)$$

$$E_{co} = K\left[\frac{A}{(s+j\omega)} + \frac{B}{(s-j\omega)} + \frac{C}{(s+\alpha+j\omega)} + \frac{D}{s+\alpha-j\omega}\right] \quad (30)$$

$$K = \frac{I_f \Omega \sqrt{3}\ L_{fa_2}}{L_t C_o}$$

$$A = \frac{-L_t}{R(2\sqrt{L_t C_t} + j\, R/2L_t)} = B \text{ conj}$$

$$C = \frac{L_t}{R(2\sqrt{L_t C} - jR/2L_t)}$$

$$D = \frac{L_t}{R(2\sqrt{L_t C} + jR/2L_t)}$$

The time domain response therefore consists of a sum of a damped sinusoid plus an undamped sinusoid.

Comparison with Undamped Case

For the undamped case it can be shown (10)(11) that this voltage across the capacitor increases by a quantity $\frac{\pi K}{\omega^2}$ at each succeeding positive or negative peak. The effect of damping, $\alpha \neq 0$, in the Equation (3 0) is to decrease this rise since the α turn corresponds to multiplication by a decaying exponential in the time domain of the steady state sinusoidal turn. If the damping is negligible, there is little effect on the first few peaks of the time domain response of the a.c. resonant waveform. The criteria for negligible damping might be defined as that value of α corresponding to a damping ratio of one tenth.

$$D = \frac{R(2L_p^2 + 3\alpha\Sigma L_p^2)}{}$$

$$C = \frac{R(2L_p^2 - 3\alpha\Sigma L_p^2)}{}$$

The time domain response therefore consists of a sum of a damped sinusoid plus an undamped sinusoid.

Comparison with Undamped Case

For the undamped case it can be shown (13)(11) that this voltage across the capacitor increases by a quantity $\frac{\pi}{\omega_c^2 L}$ at each succeeding positive or negative peak. The effect of damping, $\alpha \neq 0$, in the equation (3 0)is to decrease this rise since the α term corresponds to multiplication by a decaying exponential in the time domain of the steady state sinusoidal term. If the damping is negligible, there is little effect on the first few peaks of the time domain response of the R.C. resonant waveform. The criteria for negligible damping might be defined as that value of α corresponding to a damping ratio of one tenth.

(11)

$$\frac{\frac{R_i}{2L_t}}{\frac{1}{\sqrt{LC_{t_o}}}} = .1 \qquad \frac{R_i\sqrt{LC_{t_o}}}{L_c} = R_i\sqrt{\frac{C_o}{L_t}} \tag{32}$$

$$R \leq .1\sqrt{\frac{L_t}{C_o}}$$

The Intermediate Discharge Circuit

The instant the first saturable core goes into saturation the piecewise linear circuit of intermediate discharge, shown in Fig. V, applies. The function of this circuit is to transfer the energy of the charged C_o to the Pulse Forming Network; not only must this charge be transferred, but it must be transferred in a minimum amount of time, consistent with limitations imposed by the delay line which forms the PFN. The reason that this minimum of rise time is specified is that it is desired to keep the number of turns on the second saturable core to a minimum. If it is remembered that the impedance of this second wound core is proportional to the square of the number of turns, it can be seen that a large impedance will cause pulse distortion. A faster rise time permits fewer turns for the same voltage peak. The lumped capacitance of the PFN, $5C$, is substituted for its

five stage distributed capacitance C, a substitution which is valid when the major frequency components of the charging wave form are well below the "cut off" frequency of the artificial transmission line given by:

$$f_{co} = \frac{1}{\pi\sqrt{LC}}$$

L = inductance per stage
C = capacitance per stage (33)

Note that the current consists of that portion contributing to PFN charging and a second term, I_{sc2}, the magnetizing current passed by the second core, due to its low impedance. The mechanism of this transfer is understood by reverting to LaPlace notation; for purposes of simplicity the magnetizing current of SC2 is considered constant:

$$H_c = \frac{NI_m}{\ell_m} \quad (34)$$

$$I_m = \frac{\ell_m H_c}{N} = I_{sc2} \quad (35)$$

where: $H = H_c$, the coercive force

N = number of turns

I_m = mean core length (cm)

I_m = "magnetizing" current in amperes for the second core

$$E_{pfn} = \frac{1}{s5C}\left(I - \frac{I_m}{s}\right)$$

$$-\frac{E_{cop}}{s} + \frac{I}{sC_o} + I_g L_s + \frac{I - \frac{I_m}{s}}{5sC'} = 0 \qquad (36)$$

$$I = \frac{1}{sL_s - \frac{1}{sC'}}\left[\frac{I_m}{5s^2C} + \frac{E_{cop}}{s}\right]$$

$$\frac{I_m}{5s^2C}\left\{\frac{s/L_s}{s^2 + \frac{1}{L_sC'}} + \frac{E_{cop}\,5SC\,(s/L_s)}{5s^2C\left(s^2 + \frac{1}{L_sC'}\right)}\right\}$$

$$\mathcal{E}_{pfn} = \frac{I_m}{5CL_s s(s^2 + \omega'^2)} + \frac{E_{cop}}{L_s(s^2 + \omega'^2)} - \frac{I_m}{5Cs^2}$$

where: B = B$_{pole}$ magnetic force

ℓ_g = length of curve

ℓ_c = mean core length (cm)

I_m = "magnetizing" current in amperes for the second core

$$B_{pole} = \frac{\mu_0 N}{\ell} (I - I_m)$$

$$-\frac{\ell}{\mu_0 A_c} + \frac{\ell_g}{I} + \frac{\ell_c}{\mu_0 \mu_r A_c} + \frac{2\pi r}{I - I_m} = 0 \qquad (36)$$

$$I = \frac{\mu_0 \ell - I}{\frac{\ell}{\mu_0 A_c} + \frac{\ell_g}{I}} \left[\frac{2\pi r}{N} \right]$$

$$\left\{ \frac{2\pi r \mu_0}{I^2} \right\} \left\{ \frac{I^2 \ell_g}{\ell_g + \frac{I^2}{I}} + \frac{\cos^2 \theta \, (\ell_g + \frac{I^2}{I})}{\sin (\ell \mu_r)} \right\}$$

$$C_{th} = \frac{2\pi I^2 (\ell_g + \mu_r \ell)}{I^2} + \frac{I^2 (\ell_g + \mu_r \ell)}{\cos \theta} - \frac{2\pi r^2}{I \mu_r}$$

$$E_{pfn} = \frac{1}{s5C}\left\{I_m\left(\frac{1}{s} + \frac{1}{s5CL_s(s^2+\omega^2)}\right)\right\} + \left\{\frac{E_{cop}}{L_s(s^2+\omega 2)}\right\} \quad (37)$$

$$\omega' = \frac{5C + C_o}{L_s\, 5CC_o}$$

where L_s = saturated inductance of first core

$5C$ = lumped C of PFN

I = La Place transform of current in inductance

E_{pfn} = La Place transform of PFN voltage

In the time domain this voltage is:

$$e_{pfn}(t) = E_{cop}\frac{C_o}{C_o+5C}\left(1 - \cos\omega' t\right) - \frac{I_m}{(5C)^2}\left(5C - \frac{5C_oC}{C_o+5C}\right)t$$

$$- \frac{I_mC_o\,\pi}{5C\,(C_o+5C)}\sin\omega' t \quad (38)$$

This voltage maximizes at $t = \frac{\pi}{\omega'}$ seconds which is, of course, the time at which it is desired to have the second core saturate.

$$\int \frac{\omega^2 \, d\omega}{\left(\omega^2 + \omega_1^2\right)^2} \left\{ \frac{1}{\omega^2 + \omega_1^2} + \left(\frac{1}{\omega^2} + \frac{\omega_1^2}{\omega^2 \left(\omega^2 + \omega_1^2\right)} \right) \right\} \qquad (38)$$

The term ω' is of the order of 10^5 rad/sec and this fact gives justification for dropping out the last two terms of Equation (38) if the time interval considered is small ($\pi \times 10^{-5}$/sec). The magnitude of this first peak is:

$$E_{pfnp} = 2 E_{cop} \frac{C_o}{C_o + 5C} \tag{39}$$

From conservation of energy, for complete energy transfer:

$$\frac{1}{2} C_o (E_{cop})^2 = \frac{1}{2} 5C (E_{pfnp})^2 \tag{40}$$

$$C_o = \left(\frac{2C_o}{C_o + 5C}\right)^2 \times 5C$$

$$C_o = 5C \tag{41}$$

The Final Discharge Circuit

The saturation of SC2 effectively puts a matched termination across the charged artificial transmission line.

Since the reflection coefficient is zero at the magnetron end and unity for the open end, a rectangular pulse of duration $2 \times 5 \times \sqrt{LC}$ seconds, is delivered to the magnetron, of amplitude $\frac{1}{2} E_{cop}$ volts. The pulse transformer is assumed ideal and the impedance of the second core is assumed zero.

Due to stray capacitive effects, spurious oscillations occur if the damping diode is not placed in the magnetron circuit. The diode causes these oscillations to dampen out.

The apparent resistance that the magnetron presents is determined by the operating point set by the pulse of voltage. This apparent resistance is sketched in Fig. V. This resistance is reflected across the turns of the pulse transformer.

The output of the magnetron is led to a matched 7/8" coaxial line which is in turn matched to a resistive load.

CHAPTER III

RESULTS

The modulator system design procedure is given in Appendix II. A schematic of the overall system is presented in Fig. XV. Photographs of individual components are presented in ensuing figures.

Results and curves of data will be presented for these individual system components in the order in which they were taken. Explanatory comment is included as to the means of measurement, for the purpose of evaluating the data.

Open Circuit-Short Circuit Characteristics

These two curves are plotted against field current in Fig. VI. for various speed levels in the modulator. Speed was measured by using a GR Type 631B Strobotac which was calibrated against a Tectronix Type 514D oscolloscope. The voltages were measured with a Voltohmyst WV97 A electronic voltmeter and currents were measured with this meter across a fixed 10 ohm resistor. The object of the E_{oc} plot is to

[illegible]

The equilateral square design parameter is given in appendix D. : schematic of the overall system is presented in fig. D2. Interconnection of individual components are presented in drawing figures.

Results and scores of data will be presented for these individual system components in the order in which they were taken. Supplementary comment is included as to the cause of inconsistency, or the purpose of evaluating the data.

[illegible] Circuit Characteristics

Three bus scores are plotted against field current in fig. VI. The various speed layouts in the modulator, speed was measured by using a DC Type GJJP Tachometer which calibrated against : Instronic Type 3JJ- oscilloscope. The voltages were measured with a Voltohmyst 4VT : electronic voltmeter and currents were measured with thin outer screen a flood it dim regulator. The object of the [illegible] plot is to

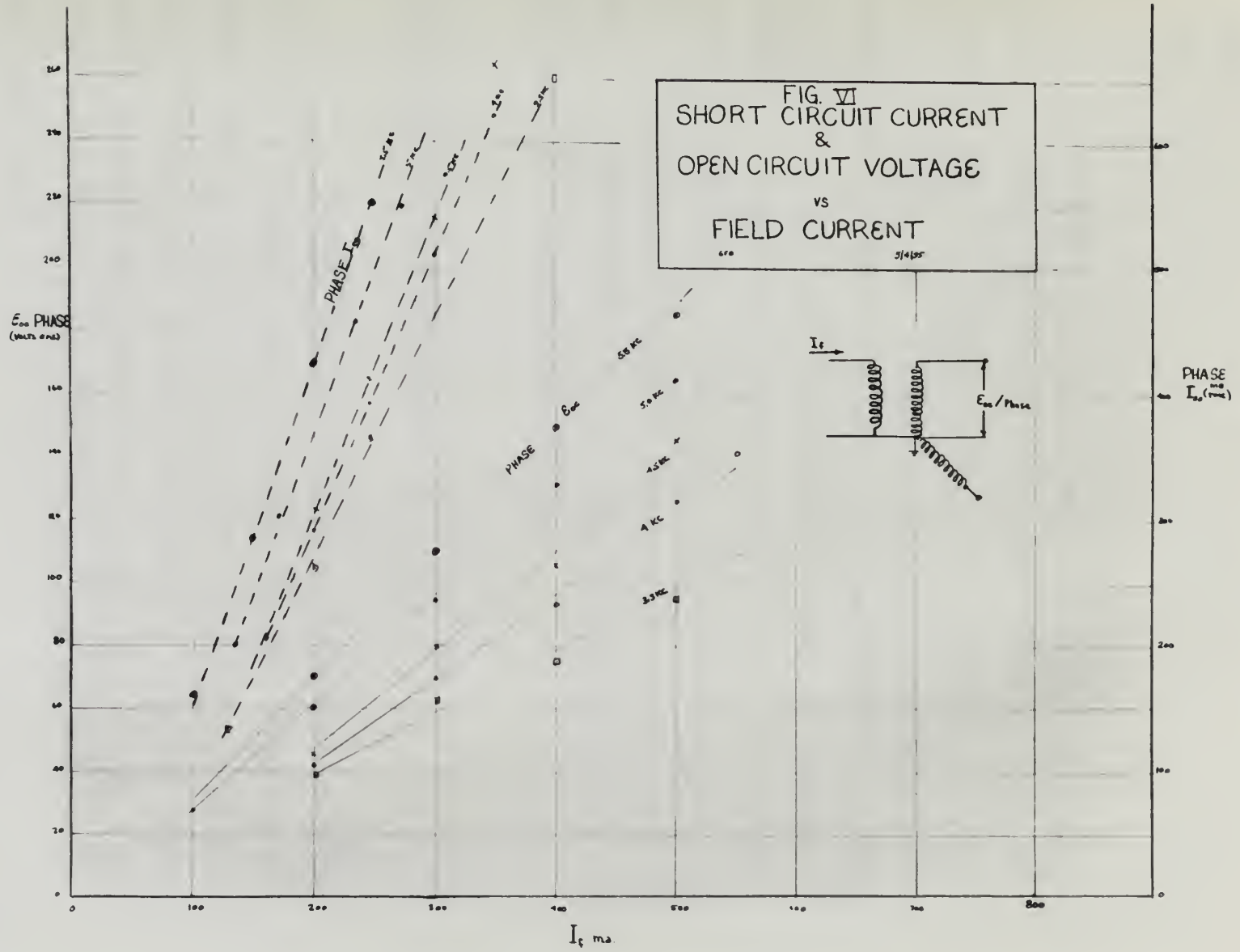
FIG. VI
SHORT CIRCUIT CURRENT
&
OPEN CIRCUIT VOLTAGE
VS
FIELD CURRENT
5/4/55
PHASE
PHASE
5.5 KC
5.0 KC
4.5 KC
4 KC
3.5 KC
I_f
E_{oc} / Phase
E_{oc} PHASE
PHASE I_{sc}
I_f ma.

measure the mutual of the field with respect to one phase belt. Phase voltages were observed to be balanced within small measurement errors. The field was excited by a constant current source. In all cases the field was oscillated for the purpose of obtaining as near a value of zero as feasible for the induced voltage, due to residual magnetism in the stator. It was observed that the residual magnetic effect for the voltage across both phases could be as high as 200 volts at 5 kc. This residual effect is noticed in that all curves cannot be extrapolated to the same point; note the irregular spacing. The object of the I_{sc} plot is to establish the synchronous impedance caused by R_1 and L_1. This was measured over an operating range near 5 kc to give an index as to damper bar effects.

Inductive Effect of One Phase

Figure VII shows a plot of the inductive effect of various windings due to the angle variant component of inductance, at 5 kc. The plot gives an index as to steady state evaluation of armature constants. A constant current source provided excitation for one phase belt of the stator, while the rotor moved at the speed corresponding to 5 kc. The alternating voltage generated in the armature was measured. This was found to be a second harmonic component solely .

an index as to degree for effects.

This was assumed over an operating range down 3 db to find to establish the electronic impedance caused by g^1 and C^1. note the theoretical curves. The object of the 1st plot is that all curves cannot be extrapolated to the same point on left axis at 2 ke. This residual effect is noticed in the plots. It was observed that the residual capacitive effect for the voltage curves both phases could be as high

Inductive Effect of One Plate

Figure VII shows a plot of the inductive effect of various shunting due to the eight various components of inductance, at 2 ke. The plot gives an index as to steady state evaluation of resistance contribution. A constant current source provided ventilation the one plate half of the electro, while the meter moved at the speed corresponding to 2 ke. The alternating voltage measured in the equations was measured. This was found to be a second harmonic component chiefly.

FIG. VII

Θ-VARIANT INDUCTIVE EFFECT OF ONE PHASE 5 KC

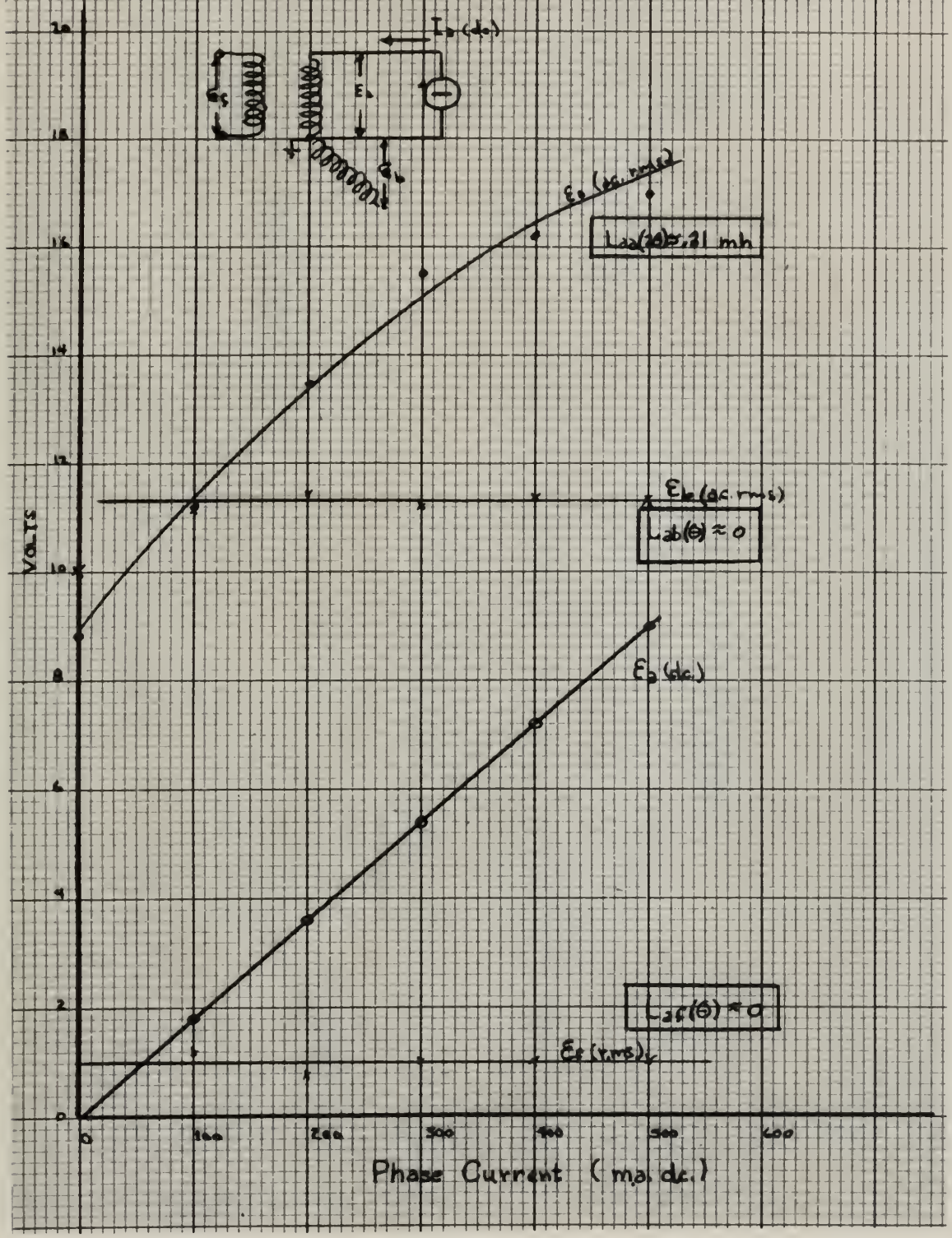

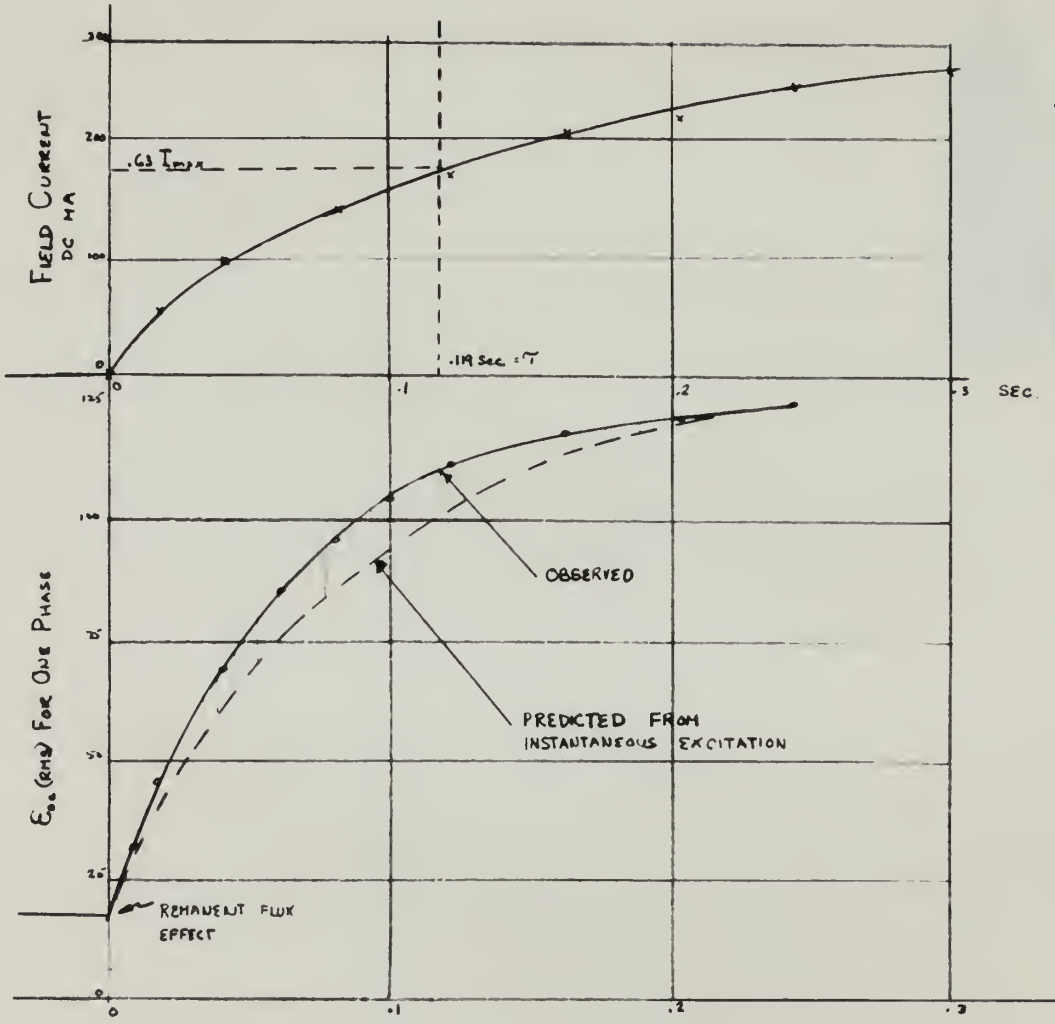

FIG. VIII
RESPONSE OF ONE PHASE
TO FIELD STEP (5 kc)

5/1/55 GFR

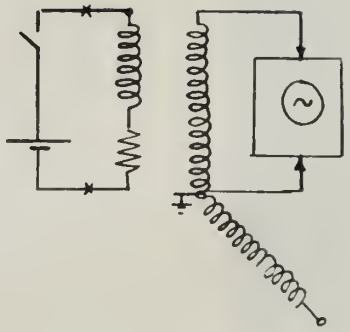

FIG. IX
TRANSIENT WAVEFORMS

5/1455 C.F.B.

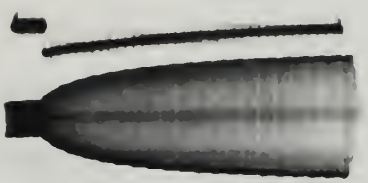

Note the magnitude of the second harmonic effect. No field voltage change was observed nor was any voltage change observed in the second phase belt.

Transient Effects

The effect of a step of voltage on the alternator field as felt by one phase belt is shown on Fig. VIII and Fig. IX. A time constant of .119 seconds was observed at 5 kc. A full load short circuit current test was made and the waveforms of this are displayed with those of the field transients, on Fig. IX. The actual photostat copies are poor in the respect that for the field step it was desired to place both voltages on the same time scale. Since the alternator output has a frequency of 5 kc, the armature waveform is blurred. In the case of the short circuit current test, the waveforms were placed on a fast sweep on the Dumont 322 oscilloscope in order to retain the identity of the armature waveform. However, the film speed was not sufficiently fast to register the waveform distintly for reproduction. For this reason the peaks have been sketched over for clarity. A time constant of about 150 μs was noted for a group of photographs. This figure was computed by assuming complete decay in five time constants. More quantitative data on short circuit response would indicate a more sophisticated technique in phasing sweep and switch

note the magnitude of the second harmonic effect. No field voltage change was observed nor was any voltage change observed in the second phase belt.

Transient Effects

The effect of a step of voltage on the alternator field as felt by one phase belt is shown on Fig. VIII and Fig. IX. A time constant of .115 seconds was observed at 5 ~~cs~~. A full load short circuit armature test was made and the waveforms of this are displayed with those of the field terminals, on Fig. IX. The normal fundamental copies are poor in the respect that for the field step it was desired to place both voltages on the same time scale. Since the alternator output has a frequency of 5 ~~cs~~, the armature waveform is altered. In the case of the short circuit armature test, the waveforms were placed on a fast sweep on the Dumont 322 oscilloscope in order to reveal the identity of the armature waveform. However, the film speed was not sufficiently fast to reclaim the waveform distinctly for reproduction. For this reason the peaks have been sharpened over for clarity. A time constant of about 150 ~~ms~~ was noted for a trend of photographs. This figure was accepted by assuming complete decay in five time constants. Here a more sophisticated mechanism in figuring speed and weight quantitative data on short circuit response would indicate

FIG X
HARMONIC CONTENT

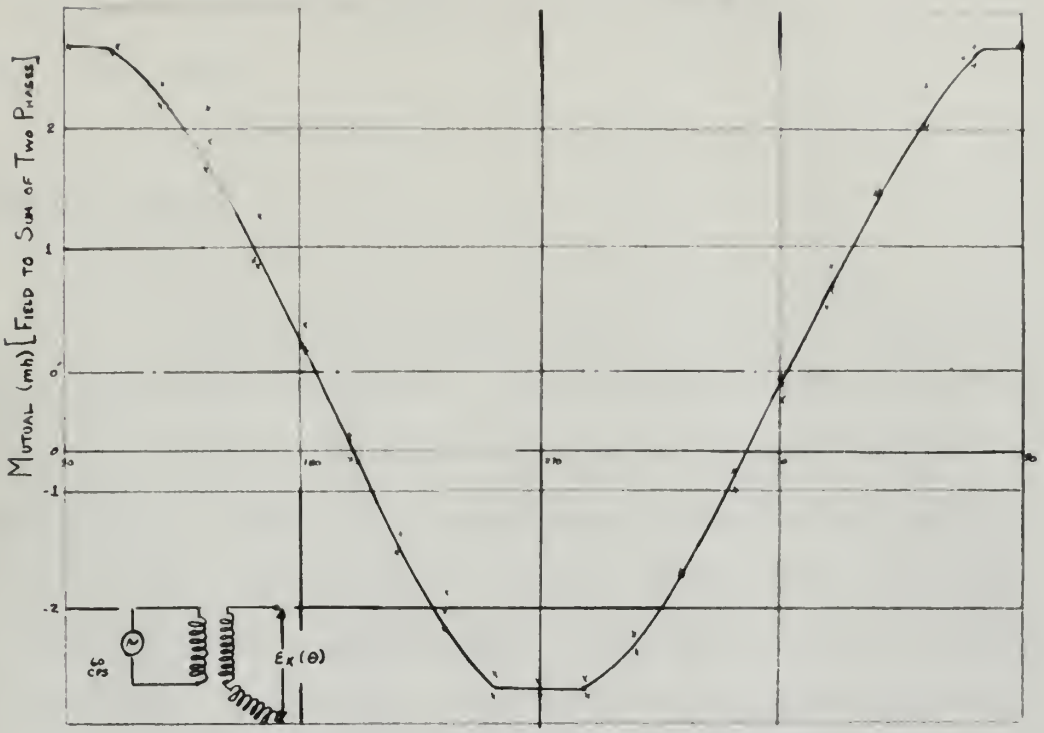

(a) 60 CPS STATIC MUTUAL OF BOTH PHASES AS A FUNCTION OF ROTOR POSITION

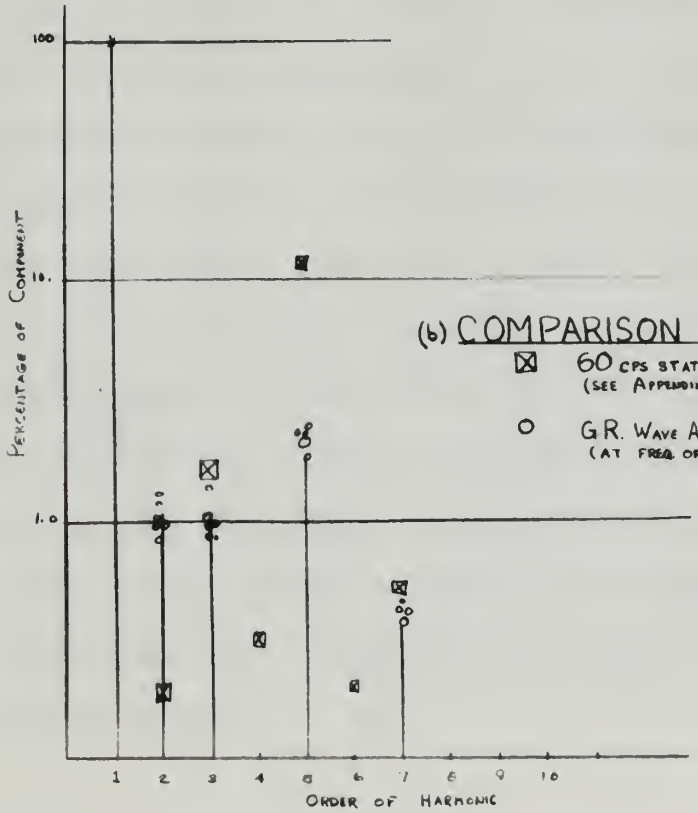

(b) COMPARISON HARMONIC CONTENT

⊠ 60 CPS STATIC MUTUAL (SEE APPENDIX I, ROLFE'S SCHEDULE)

○ G.R. WAVE ANALYZER TYPE 736A (AT FREQ OF FUNDAMENTAL < 2 KC)

closure times. A DPST switch was used here within one pole was displaced so as to trigger the sweep before the short circuit was made.

Harmonic Content

A 60 cycle "static" test of field to armature mutual inductance was made. The resulting curve is shown in Fig. X. Both phase belt voltages were used in the computation of this mutual which is a function of rotor position. This is termed a "static" test since the rotor was held fixed at a known angle while the armature voltage was measured. The mutual inductance is derived from this term. An analysis for harmonics was performed by numerical methods and this procedure is given in Appendix I. The fifth harmonic is the most pronounced at the static test, having a magnitude of about 11% of the fundamental. A separate "dynamic" analysis was performed using the GR Wave Analyzer, Type 736-. This has an upper limit on frequency 16 kc, hence it was necessary to operate below 3 kc for harmonic determination. It was first assumed that the waveform would be a function of rotor displacement. A comparison of the results of the two means of measurement is given in Fig. X. In general the static harmonics are higher, than when the measurements were taken with the rotor turning at the fundamental frequency.

elapsed time. A 1812 Bulletin was issued twice within one pole
was displaced so as to include one sunspot before the sunspot
already was inside.

Resonance Capacity

A 60 cycle "static" test of field to armature
mutual inductance was made. The resulting curve is shown
in Fig. 4. Both phase belt voltages were used in the
computation of this mutual which is a function of rotor
position. This is termed a "static" test since the rotor
was held fixed at a known angle while armature voltage
was measured. The mutual inductance is derived from this
curve. A similar for inductance was performed by measuring
voltage and this procedure is given in Appendix I. This
field inductance is the most pronounced as the static test
during a multiplicity of about 111 of the fundamental.
Extensive "dynamic" analysis was performed using the GE
Sine Analyzer, Type 321-C. This line an output limit of fundamental
to 10, hence it was necessary to eliminate points 3 to four
harmonic distortions. It was first assumed that the sine-
form would be a function of rotor displacement. A sampling
of the results at the one degree of measurement is given in
Fig. 5. In general the static inductance was higher, since
when the measurements were taken with the rotor rotating at
the fundamental frequency.

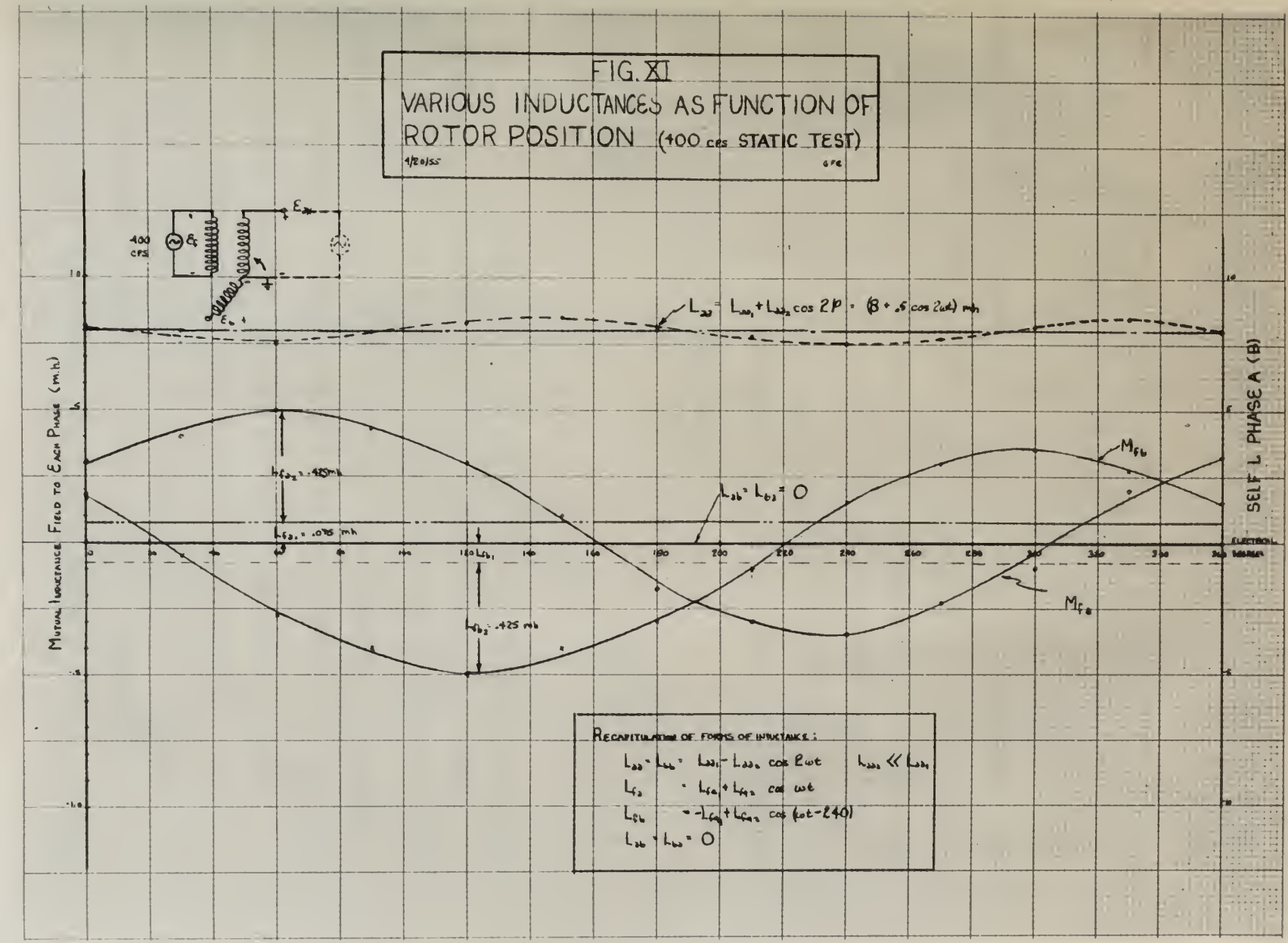
FIG. XI
VARIOUS INDUCTANCES AS FUNCTION OF ROTOR POSITION (400 cps STATIC TEST)
400 cps
$L_{aa} = L_{aa_0} + L_{aa_2} \cos 2p = (\beta + .5 \cos 2\omega t)$ mh
M_{fb}
M_{fa}
$L_{ab} = L_{ba} = 0$
$L_{fa_2} = .425$ mh
$L_{fa_0} = .075$ mh
$L_{fb_2} = .425$ mh
MUTUAL INDUCTANCE FIELD TO EACH PHASE (m.h.)
SELF L PHASE A (B)
RECAPITULATION OF FORMS OF INDUCTANCE:
$L_{aa} = L_{bb} = L_{aa_0} - L_{aa_2} \cos 2\omega t$ $\quad L_{aa_2} \ll L_{aa_0}$
$L_{fa} = L_{fa_0} + L_{fa_2} \cos \omega t$
$L_{fb} = -L_{fa_0} + L_{fa_2} \cos (\omega t - 240)$
$L_{ab} = L_{ba} = 0$

General Forms of Inductance as a Function of Rotor Position

A 400 cps "static" test was performed on the machine. The results of this test are given in Fig. XI. The purpose of the test was to verify the forms of inductances as hypothesized in Chapter II. Note that there is a constant term and a positionally-dependent term for each inductance. Note that there is no correlation in magnitude between the 60 cps static test and the 400 cps test. (In both the magnitude of exciting current was the same, 500 ma.) Note the small second harmonic waveform of the self inductance of the armature.phase belt.

Machine Losses

A summary of the losses of the machine is shown in Fig. XII. The value of full load current was chosen arbitrarily on the basis of 650 v (rms), .615 a (rms) for a 400 watts rating. Armature resistance was found to vary from about 79 ohms to 90 ohms, due to heating effects presumably. An estimated accuracy of 10% is given for these power figures. These losses were obtained by measuring the no load power consumption of the Dumore motor as a function of speed, with the resistance of the motor armature. By measuring total power into the alternator-motor system, and

General theory of behaviour as a function of force fields.

A 100 cps "static" test was performed on the machine. The results of this test are given in Fig. 11. The purpose of the test was to verify the form of impedance as hypothesized in Chapter II. Note that there is a constant term and a positively-degressive term for each instrument. Note that there is no correlation in magnitude between the DC cps static test and the 100 cps test. (In both the magnitude of unwinding movement was the same. You can note the small reversed harmonic oscillations of the hair insurance of the armature.plane- belt.

Shadow images

A summary of the images of the machine is shown in Fig. XII. The value of full load current was changed arbitrarily in the basis of (50 + (rms) .01% x(rms)for a 100 cycle motion. Armature resistance was found to vary from about 7% ohms to 90 ohms, due to heating effects primarily. A vertical recovery of 10% is given for three power figures. These losses were obtained by measuring the no load power consumption of the Sperry motor as a function of speed, with the resistance of the motor armature. By measuring total power into the alternator-motor system and

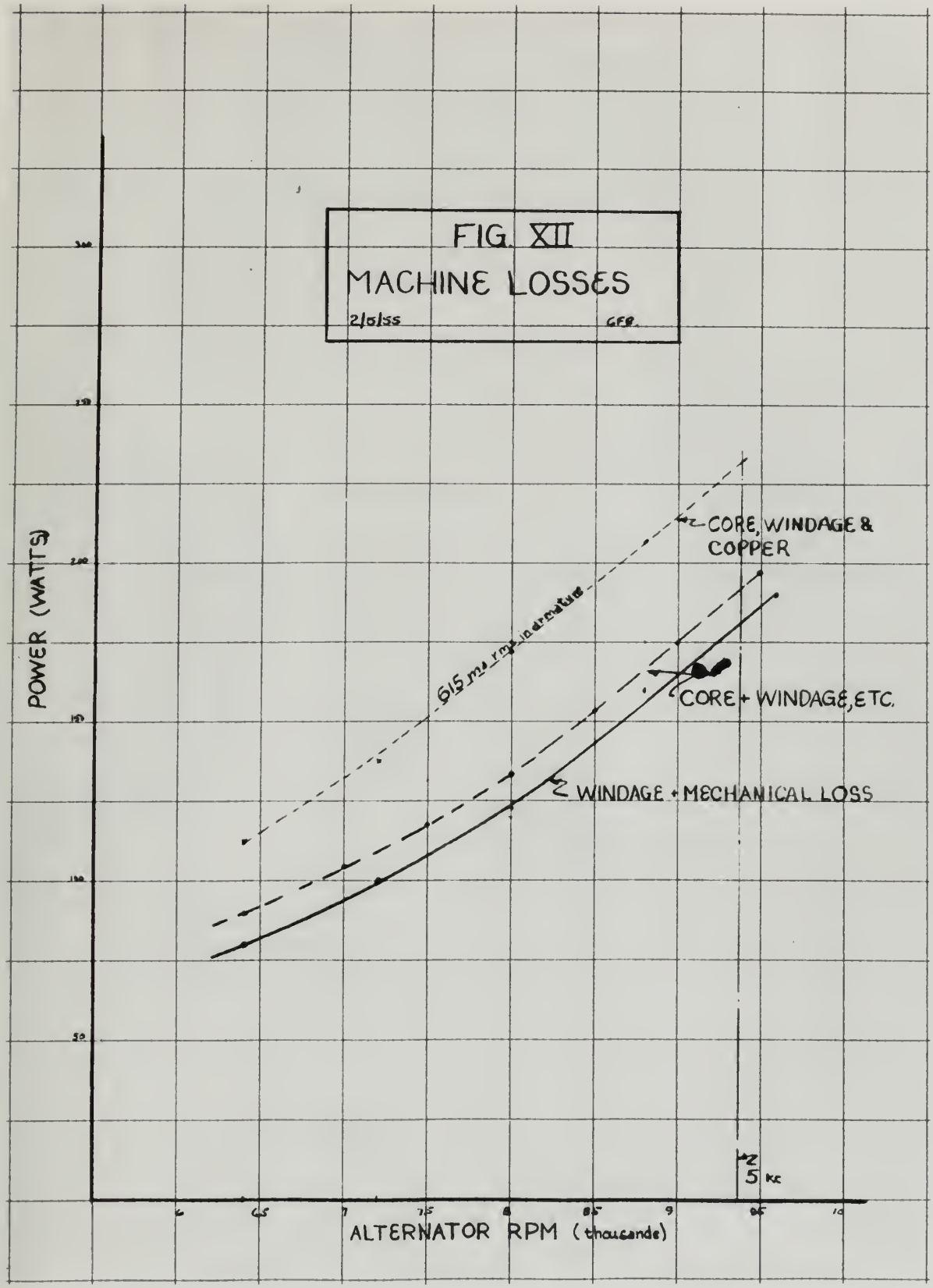
FIG. XII
MACHINE LOSSES
2/0/55
GFB.
POWER (WATTS)
CORE, WINDAGE & COPPER
615 rms rpm in armature
CORE + WINDAGE, ETC.
WINDAGE + MECHANICAL LOSS
5 KC
ALTERNATOR RPM (thousands)

FIG. XIII
HYSTERESIS LOOP

5/2/39 — Cl. A

ARNOLD 5387D1 CORE

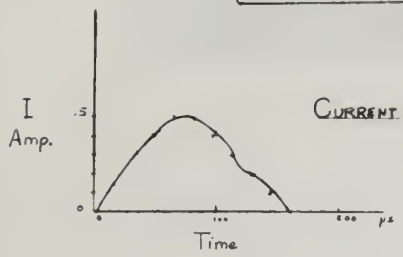

CURRENT DRIVE

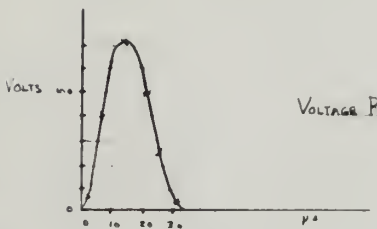

VOLTAGE RESPONSE

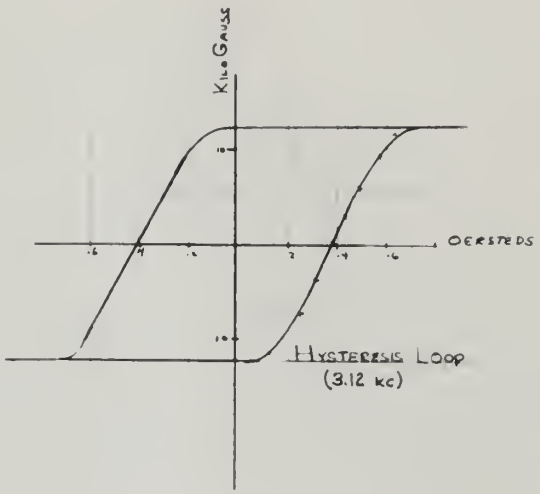

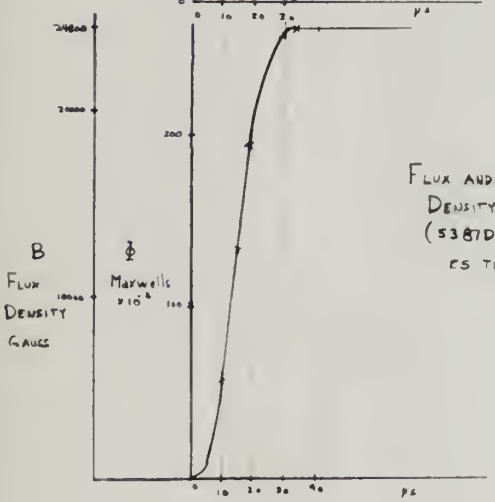

FLUX AND FLUX DENSITY
(5387D1)
25 TURNS

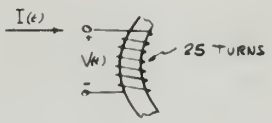

FIG. XIV

CORE RESPONSE

i (t)

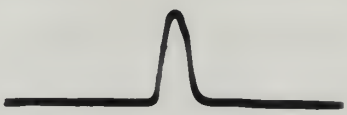

e (t)

applying motor losses, the power consumed by the alternator was attained.

Hysteresis Loop Measurement

An example of the method used to measure hysteresis loop constants at frequencies near 5 kc is shown in Fig. XIII. The core was current driven from the alternator. Voltage and current waveforms were taken (Fig. XIV). These were translated into the B-H Characteristic. A somewhat low value for maximum flux density was measured on the first stage core, using this method. Saturated permeability values were taken by biasing the core into saturation by means of a bias winding and by measurement of the impedance developed by this winding.

Final System

Based upon the evaluation of constants illustrated in the foregoing, and upon the modulator design procedure contained in Appendix II, a magnetic modulator was fabricated for operation from a 5 kc pulse repetition frequency. The system schematic is illustrated in Fig. XV. A Binks air compressor furnishes a supply for the oil mist system. The charging capacitor, C_o, is .0075 μf. This is charged by the inductor alternator through an external inductor, 130 mh. The first stage core, an Arnold 5387D1, is wound with 709 turns of #18 heavy formvar insulated copper wire. The bias winding is 50 turns of #10 heavy formvar insulated copper wire.

applying wave theory. The power consumed by the alternator was studied.

Determining Loop Impedances

An example of the method used to measure input-terminals loop conductance at frequencies near 5 Mc is shown in Fig. XIII. The note was observed twice: once from the alternator. Voltage and component measurements were taken (Fig. XIV). These were transformed into the set's parameters. A nomograph for various flux densities was measured at the first stage core, using this method. Measured permeability values were verified by placing the core into saturation by means of a bias winding and by measurements of the inductances developed by this winding.

Final Design

Based upon the evaluation of experimental circuits tested in the laboratory, and upon the satisfactory design procedure mentioned in Appendix II, a complete oscillator was fabricated for operation from a 5 mc quartz crystal frequency. The crystal commercial is illustrated in Fig. IV. A diode air compressor regulates a supply for the bit rate system. The clocking equation, $e_{ck} = .005 \sin \omega t$. This is charged by the inverter alternator through an external inductor, 130 mh. The first stage core, in model 5307J3, is wound with 750 turns of #42 heavy Formvar insulated copper wire.

FIG. XV
SYSTEM SCHEMATIC

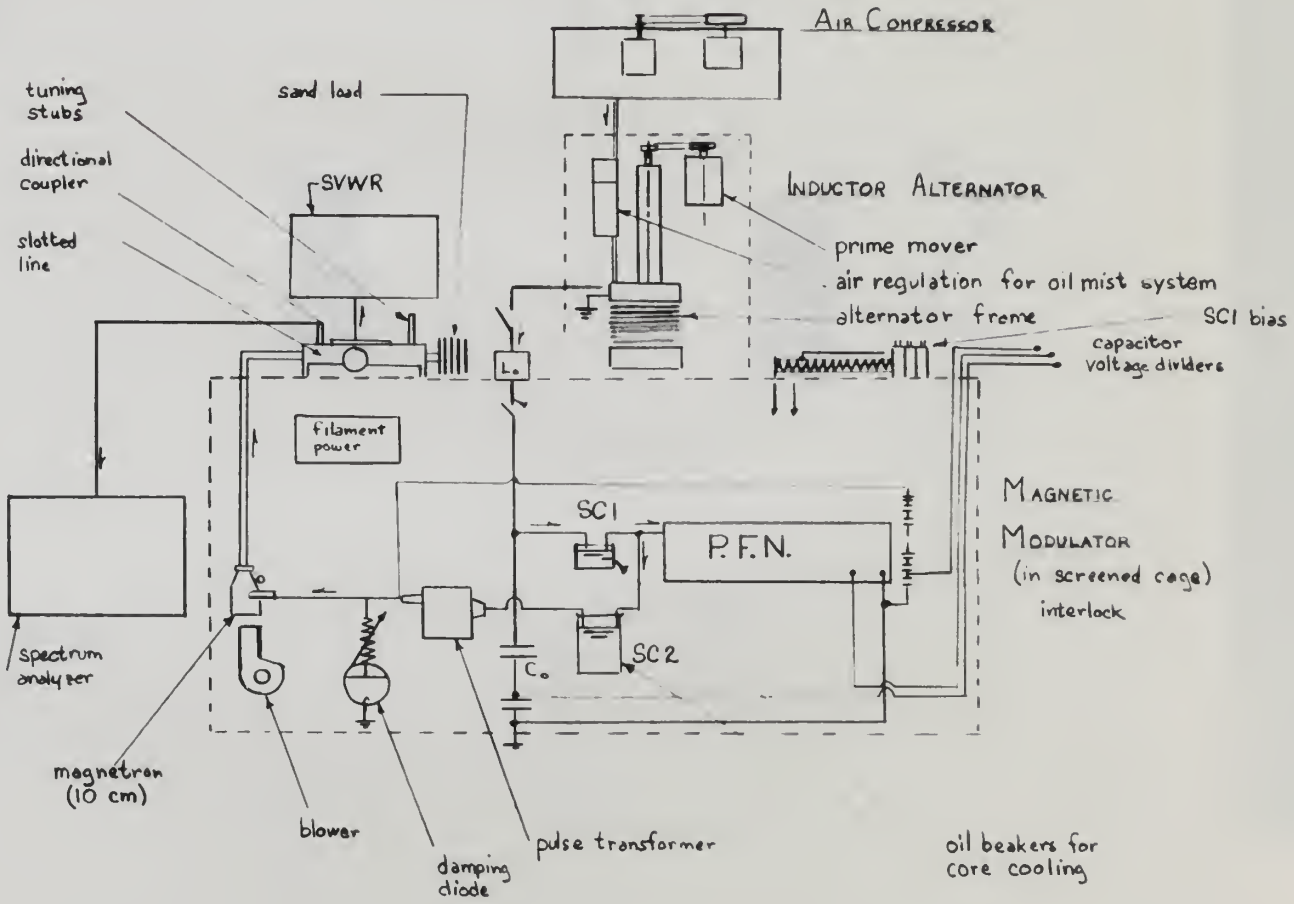

FIG. XVI
MODULATOR WAVEFORMS

5/16/55 GJR

$\mathcal{E}_{CO}(t)$

(1)

(2)

$\mathcal{E}_{PFN}(t)$

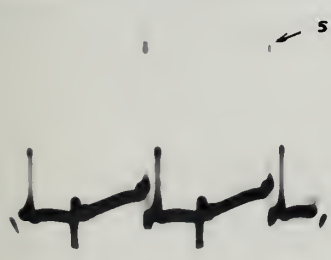

$\mathcal{E}_{MAG}(t)$

The delay line inductance is 6.65 μh and the capacitance is .0015 μf. The second stage saturable core consists of 8 stacked 50003 Orthonol cores wound with 70 turns of #18 H.F. copper wire.

Waveforms observed with the modulator are shown in Fig. XVI. Excitation was 700 ma. Peak values of voltage were measured across voltage dividers made up of series capacitors. The voltage dividers were calibrated with a Hewlitt Packard Pulse Generator on a Tectronix 514D scope. It will be noted that the first core is saturating prematurely. Bias current on the first saturable core was .71 amperes. A spectral analysis of the magnetron output was attempted using a Type 107 Spectral Analyzer (Sylvania). The spectrum was quite unstable and was not photographed for this reason. A standing wave voltage ratio of 1.05 was observed using a TS-12/AP Standing Wave Indicator.

Detailed photographs are listed on figures following Fig. XVII which point out details of components.

The delay line inductance is 6.65 and the capacitance is .0025 μf. The second stage saturable core consists of 5 stacked 50003 Permalloy cores wound with 70 turns of #18 E.N. copper wire.

Waveforms observed with the modulator are shown in Fig. XVI. Excitation was 700 cps. Peak values of voltage were measured across voltage dividers made up of surface capacitors. The voltage dividers were calibrated with a Dumont Peaked Pulse Generator on a Tektronix 525 scope. It will be noted that the first core is saturating prematurely. Bias current on the first saturable core was .71 ampere. A spectral analysis of the capacitor output was attempted using a Type 107 Spectral Analyzer (Hyfrequ). The spectrum was quite unstable and was not photographed for this reason. A steadier wave voltage ratio of 1.02 was observed using a TS-12/AP Ballistic Wave Tabulator.

Detailed photographs are listed on figures following Fig. XVII which point out details of components.

CHAPTER IV

DISCUSSION OF RESULTS

Open Circuit-Short Circuit Characteristics

From the value of open circuit voltage per phase, Fig. VI, it is found that a per phase mutual of 15.2 mh applies over the range 3.5 kc to 5.5 kc. This value is constant within the tolerances of measurement errors, estimated at 5%. From the values of I_{sc} and E_{oc} can be found an impedance made up of internal constants of the armature. If it may be allowed to skip to the value of internal resistance, 80 ohms, obtained from power input measurements, it is found that the apparent self inductance of one phase increases from 3.3 mh at 3.5 kc to 4.2 mh at 5.5 kc. Since the second harmonic component of the self inductance is assumed negligible (to be verified) it is assumed that this rise of 25% in the value of self inductance, is due to the effect of damper bar coupling.

Time Variant Inductance of One Phase

A straight line approximation for the self inductance of an armature phase was made for the case of the second harmonic component of L_{aa}, namely L_{aa2}. This gave a value for this term which was 7.5% of that of the constant self inductance. The net inductive effect would be 15% since it is a second harmonic term. Hence, it is felt that the omission

Time Varient Inductance of One Phase

A graphic time approximation for the self inductance of an armature phase was made for the case of the assumed harmonic component of L_{aa}, namely L_{aa2}. This gave a value for this term which was 7.5% of that of the constant self inductance. The net inductive effect would be 15% since it is a second harmonic term. Hence, it is felt that the mutation

of this term is justified for first order purposes.

Transient Effects

The inductance of the field winding was determined to be .27 henry. Its zero frequency resistance was 35 ohms. This gives a predicted time constant for the winding of .0077 sec. The transient observed for a step input of voltage on the field contained a time constant of .119 sec. This disparity involves a factor of 15. An explanation available here lies in the coupling due to the damper bars. This is a large problem to quantitize in the steady state condition, and is larger for the transient condition.

Sketched on Fig. VIII is the predicted waveform for the armature phase, obtained from taking the instantaneous excitation current and applying the field to phase mutual. This predicted curve falls within 10% of the plotted waveform observed, allowing for remanent flux effects. It is felt that the 10% difference is at the accuracy margin of the data.

For the short circuit current transient the time constant may be computed for an inductance of 4 mh and a resistance of 40 ohms, as .0002 sec. This value of 200 microseconds is near enough to the experimental value to lead to the observation that the internal constants of the armature

of this term is justified for first order purposes.

Transient States

The inductance of the field winding was determined to be .37 henry. The zero frequency resistance was 32 ohms. This gives a predicted time constant for the winding of .0077 sec. The transient observed for a step input of voltage on the field contained a time constant of .119 sec. This discrepancy involves a factor of 15. An explanation available here lies in the coupling due to the damper bars. This is a large problem to quantitize in the steady state condition, and is large for the transient condition.

Sketched on fig. XIII is the predicted waveform for the armature phase, obtained from taking the instantaneous excitation current and applying the flux to phase method. This predicted curve falls within 20% of the plotted waveform observed, allowing for resonant flux effects. It is felt that the 10% difference is on the measuring margin of the data.

For the short circuit current transient the time constant may be computed for an inductance of .4 ohm and a resistance of 49 ohms, or .0082 sec. This value of 500 micro-seconds is near enough to the experimental value to lend to the observation that the internal constants of the generator

winding alone govern for the case where the terminals of this winding are short circuited with zero current in them. For the case where current is in the armature at the instant of closure, a more complicated explanation is probably required due to coupling with the damper bars. In any event, it is felt as a result of these preliminary probings that if this point is of importance for some contemplated form of operation for the alternator, the dynamic response must be assessed by use of refined scope techniques which permit examination of the waveforms at intervals of 10 microseconds following closure. For the mode of operation used in a.c. transient resonant charging, the current is almost zero at the instant the first stage saturable core fires.

Harmonic Content

The "dynamic" test for harmonic content with the use of the G.R. Wave Analyzer seems to show that the damper bars have performed the intended function, namely to improve the steady state waveform.

General Forms of Inductances

The results of the 400 cps "static" test does verify the qualitative prediction of the forms of inductances made in Chapter II. Note that the phase displacement of the two mutuals, with reference to the respective constant component of each, is 120°. The value of mutual here obtained is apparently useless, since it differs from the values obtained by using other frequencies. No correlation

of the values of inductances obtained in this "static"test procedure was noticed as various frequencies were used. Indeed, the values obtained for a specific frequency varied with the level of remanent flux. For quantitative measurement of these inductances, the values of inductances were taken from the operating characteristics of the alternator.

Machine Losses

It is apparent that the machine is not too efficient (less than 64% efficiency at 5 kc full load). It might be expected that considerable heat would develop as a result of 200 watts internal dissipation at 5 kc. However, such is not the case. The oilmist system keeps a continual coolant flow, of course, and it is deduced that herein is the reason why the machine does not heat up. At no time in the course of this investigation did the alternator show signs of overheating, although both air compressor motor and prime mover motor were constantly running hot.

Method of Core Testing

This is a very interesting subject for which the reader might be rewarded by a cursory look at (9) (Production Testing of Magnetic Core Materials, AIEE Conf. Paper, 6/54)

The reason that current drive was selected here was because it was the easiest to realize; however, current drive is not a bad choice since flux drive has been criticised due to time variant random inconsistencies in repetitive operation. Since the maximum flux change is the salient item of interest in the hysteresis loop, any legitimate means would presumably give acceptable results. With regards to coercive force pre-determination, it is doubtful if the current drive produces a valid quantitative figure for this; it islikely to give a higher quantity. This pre-determination, however, is of second order importance to modulation in any event, since a well-designed circuit would provide means for adjustment of this bias. Any valid method of checking saturated permeability would also be applicable to the problem at hand.

Pulse Shape

A casual glance at the waveforms obtained in Fig. XVI will lend credence to a statement here that waveforms could stand vast improvement. A word of explanation is in order for these waveforms is in order.

The criterion to be settled first was felt to be the voltage magnitude relationship, to wit, 5 kv at the cathode of the magnetron. Therefore the excitation was adjusted to give the 5 kv peak voltage at this output.

when this was done, the volt-time integral of the waveform at C_o had exceeded the ability of the turns on SC1, the first stage core, to fire at the repetition frequency; saturation was occurring prematurely. Since firing occurred at the peak, where the first derivative has a low value, the value of 2 kv was correct. This particular core case had been burned from overheating in a previous modulator model tested earlier and it is possible that its maximum flux swing had altered since the series of test runs. It was the burning which prompted the use of oil immersion on both cores.

Therefore, there are two series of waveforms shown in Fig. XVI. The lower left two waveforms correspond to the waveform of L_{co} (t) shown at the top. These three correspond to 5 kv at the magnetron cathode. Note the premature saturation and its attendant effects reflected into following circuits.

Excitation was then reduced to 4.5 kv at the magnetron which reduction eliminated the premature saturation of SC1. The lower right hand waveforms of Fig. XVI resulted from this change. These show a pulse rise time of about .3 microseconds, a <u>flat</u> portion of about .8 microseconds and a rampliko fall off of about 1 microsecond. The last could have been steepened somewhat by trial and error tuning of stray elements. These pulses are quite satisfactory in shape, but not in peak magnitude since the reduction in voltage has placed the magnetron in the unstable region. Minor local areas

on the pulse were noted to be fuzzy perhaps as a result of the use of the eight stacked cores at SC2.

Spectral Analysis

The aim of spectral analysis had been to use the output spectrum as a criterion of pulse shape. Hence, if a spectral envelope of sine (x) / x could have been obtained with an imperfect waveform, due to net internal effects, a better index as to system performance was at hand than that given by pulse shape alone.

A standing wave ratio of 1.05 was achieved by adjustment of the termination; however no stable spectrum was retained. This is not unreasonable since it could be expected that the 5 kv voltage trigger (i.e. the left hand pulse series on Fig. XVI), contained spurious oscillations caused by the train of parasitic spikes. For the right hand set of pulses, the peak voltage is about 4.5 kv which places the operating point in the shaded area of Fig. IV. Thus it is apparent that if good spectra were to be obtained, it would be accidental.

CHAPTER V

CONCLUSIONS

From the foregoing it is concluded that:

(a) The core should be oil immersed for temperature control and stability. Melville (2) used oil immersion for both dielectric properties and for cooling on a modulator operating at 1500 cps. For a field model, this could involve packaging in a finned oil casing so that the heat dissipative surface can be proportional to volume.

(b) The inductor alternator efficiency is marginal for this speed. The basic concept of the use of the inductor alternator here is sound and practicable in the controlled-environment stage. For high frequency power generation, there appears to be potential volume gains but auxiliary bearing equipment (i.e. the air compressor should be integrated as an essential part of some other portion of the overall system, thus the bookkeeping costs and volume of this parasite system would be split.

(c) The magnetic modulator is a sound and practicable answer to the problem of radar modulation reliability

CONCLUSIONS

Thus the following is an evaluation which

(a) The model should be well developed for undergraduate content and suitability. Material (a) under the Impression for both distinctive perspective and the evolving as a foundation depending on life cycle. For a final model, this could improve particularly in a flipped all evening to find the best distinctive overview how to predominant to volume.

(b) The laboratory alternative difficulty is recycled for this phase. The basis economy by the use of the laboratory alternative have to amount and particularly in the constructive-experimental stage. The high frequency power generation there appears to be potential values using the quality learning application (i.e. the air compressed should be temperature as an essential part of some other portion of the product system, then the technology parts and values of this previous system would be split.

(c) The negligible contribution in a normal and practicable manner be the problem of lower resistance reliability

improvement. Core eccentricities at the production level might be handled analogous to present means of production calibration of the quadrature field of the G.E. amplidyne, namely the hard engineering thought embodied in the comment, "after all analyses are finished, we still have a turn or two to play with."

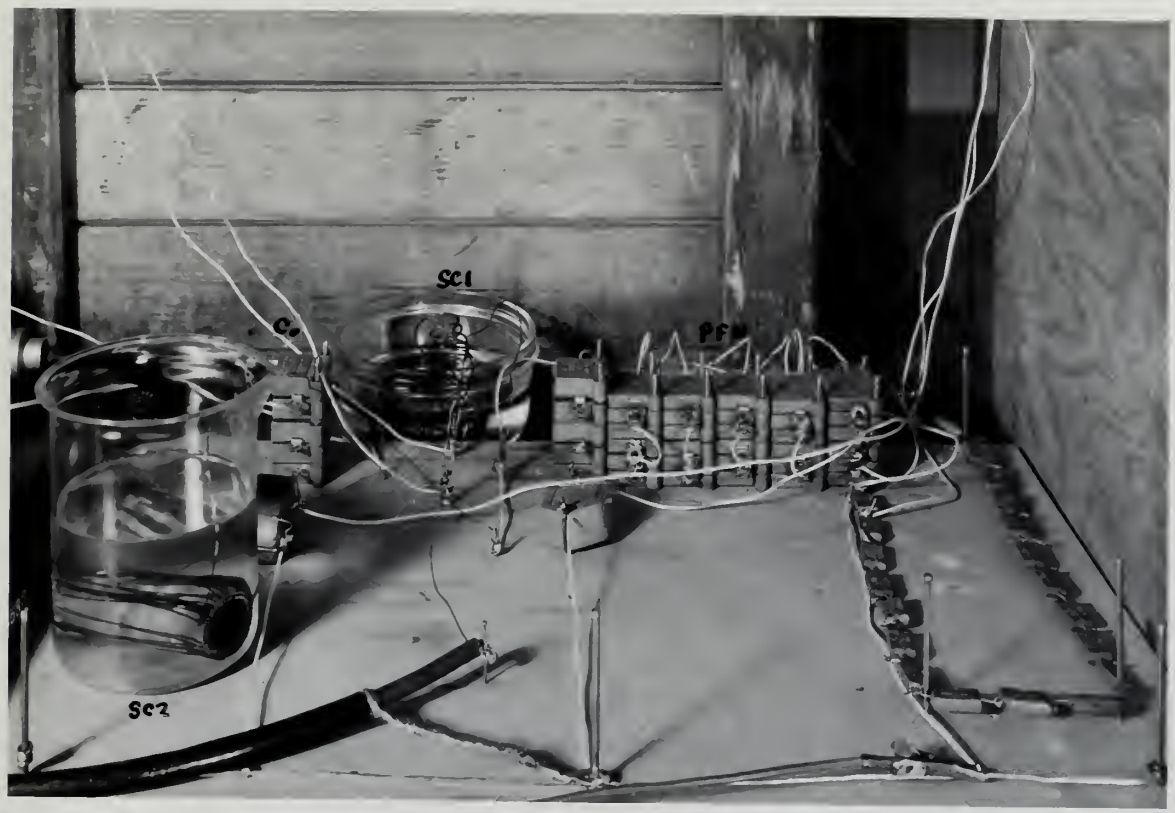

FIG. XVII

EXPERIMENTAL MODULATOR

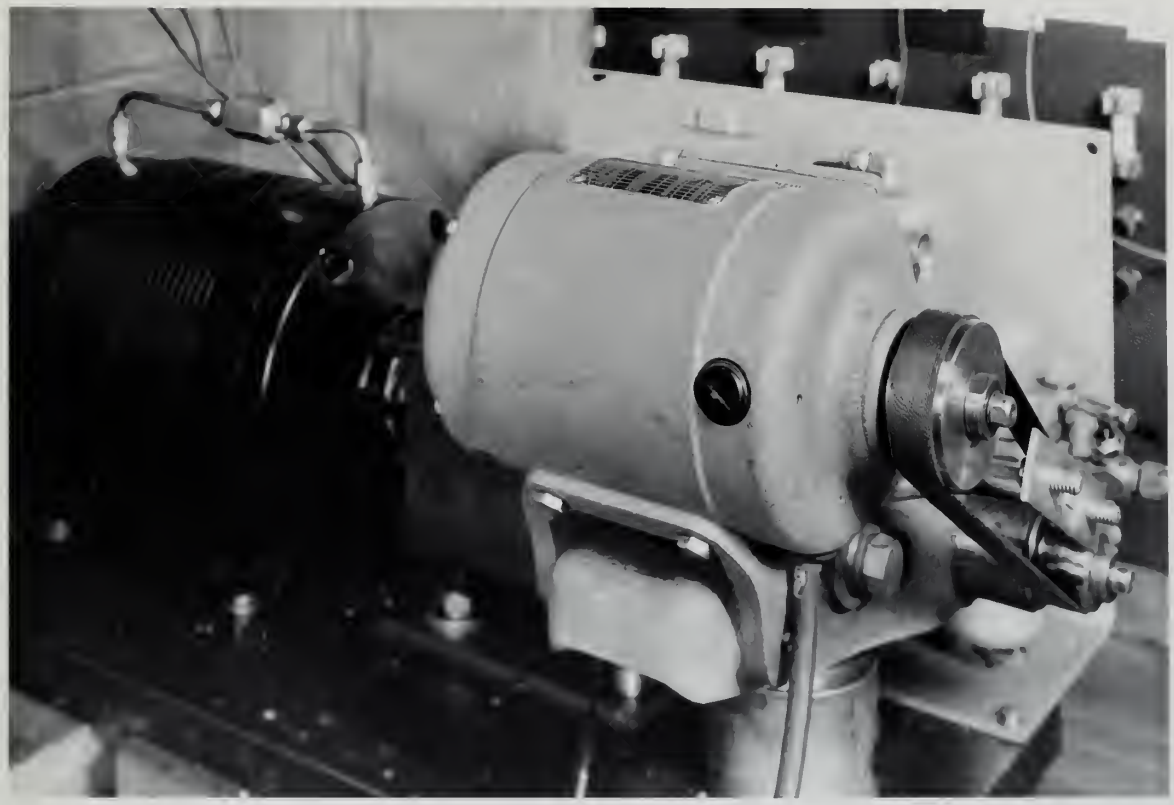

FIG. XIX

INDUCTOR ALTENATOR

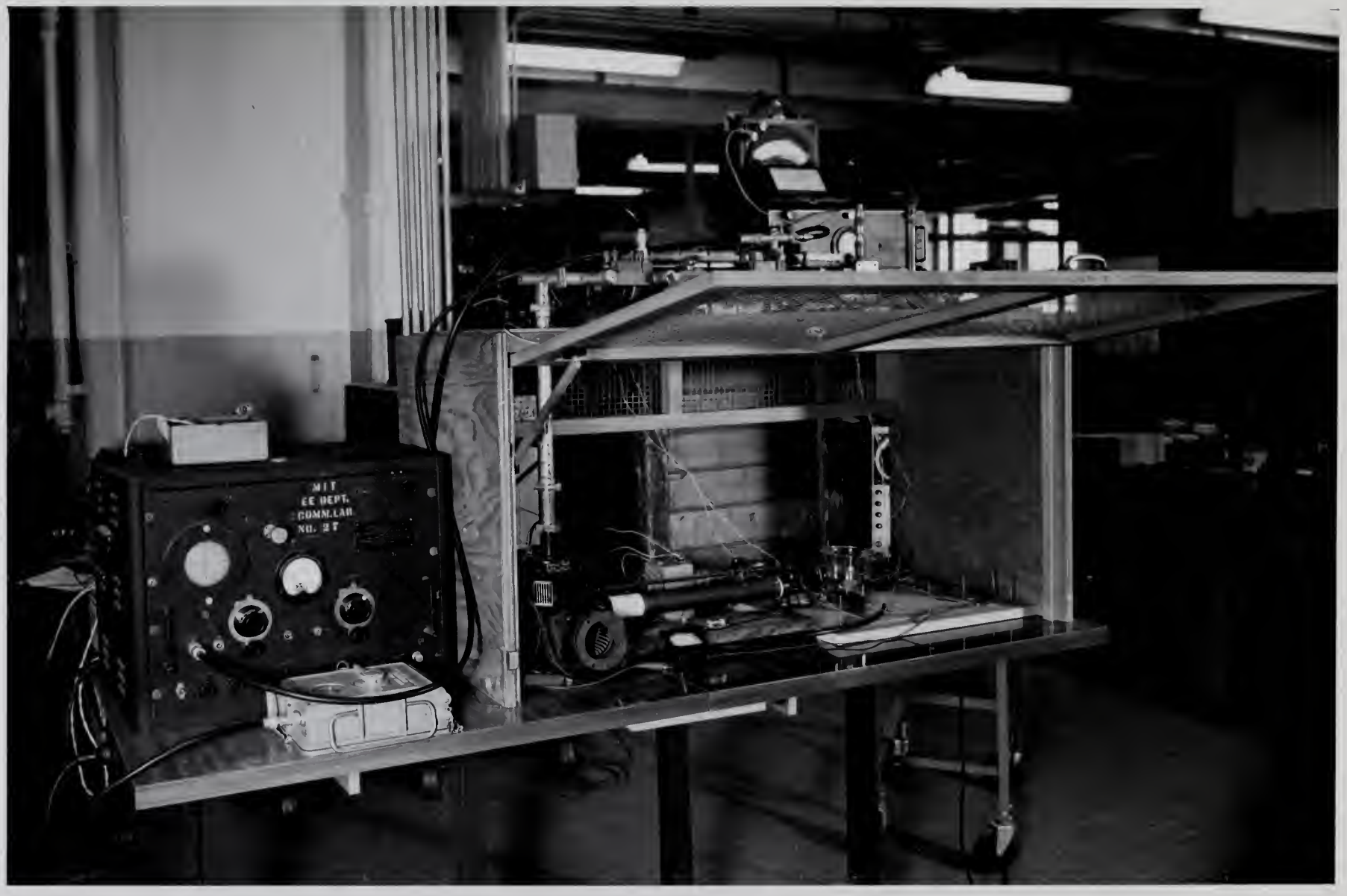

FIG. XX MODULATOR SYSTEM

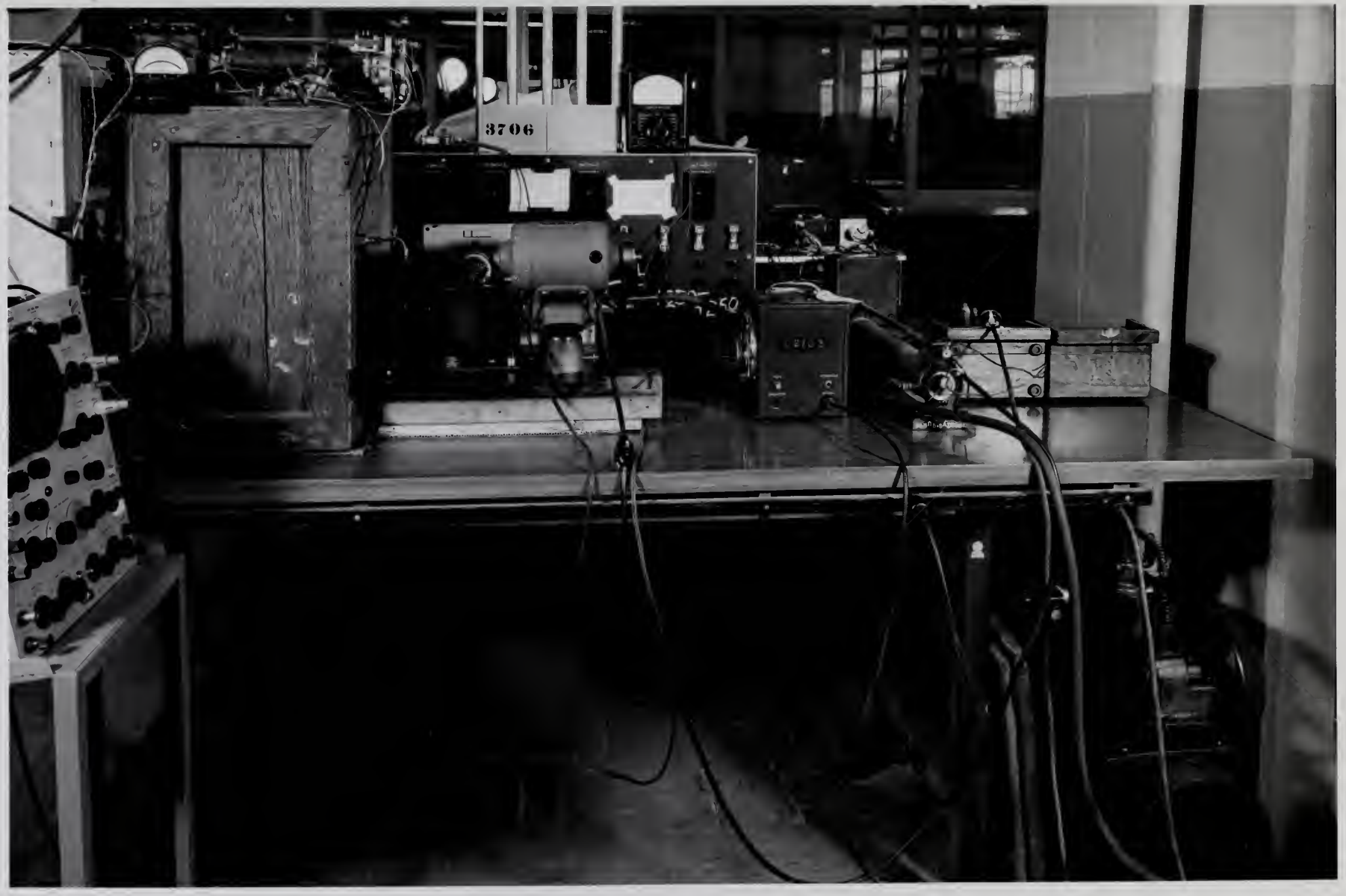

FIG. XXI POWER SUPPLY

CHAPTER VI

RECOMMENDATIONS

The following stones are a few of the many which might be turned to assist in a proper understanding of the use of this modulator system:

(a) Test run several types of square loop materials for optimization:

The use of the eight matched cores for the second stage switch may be questionable in that a cleaner pulse without minor fuzzy areas might be achieved. The use of eight cores here was for the purpose of meeting the volt-time integral requirements with the "least-inductance" solution.

(b) Refined transient data on the alternator:

The possibility of a more complex lumped parameter set of circuits exists here to account for the damper bars. Note that the disparity in the field time constants as predicted and as observed, can be caused by currents in the damper bars.

(c) Replacement of prime mover:

This includes a higher powered prime mover to enable operation at higher pulse repetition frequencies, where use of the machine would be more advantageous.

CHAPTER 13

CONCLUSIONS

The following remarks are a few of the many points which might be touched on briefly in a proper consideration of the use of this calculative apparatus.

(a) Short run numerical tricks of computing laws restricted for applications.

The use of this right weighted square for the contrac single method may be questionable in that a slightly paths different volume theory scheme might be obtained. The use of right square laws use for the purposes of testing the unit-time integral predictments with the "least-squares" solution.

(b) Optimal forecasting depending on time differentials

The possibility of a more complex lumped parameter set of dynamic models where to accommodate the time change laws. Note that the disparity in time itself cannot be predicted and be observed, can be caused by occurrence in this change laws.

(c) Development of system concept

This includes a higher dimension paths sphere to enable operation at higher pacific capabilities Correspondence, theory when of the machine should be zero adversaryness

(d) Operation at a lower duty ratio on the magnetron:
A shorter pulse width to bring the duty ratio on the magnetron down to about .001 would be desirable from practical considerations.

(d) Something to a lower duty inside on the assessment
a shorter period which is having the duty ratio on
the assessment down to about .007 would be considered
those permitted exemptions.

APPENDIX I

HARMONIC ANALYSIS OF MUTUAL INDUCTANCE OF FIELD TO BOTH PHASES (Runge's Schedule)

Ordinate Nr.	0	1	2	3	4	5	6	7	8	9	10	11	12	13	14	15	16	17	18	19	20	21	22	23
	24	41	46	45	44	43	42	41	40	39	38	37	36	35	34	33	32	31	30	29	28	27	26	25
Ordinate Value	0	1	3	8.5	12	15	11	20	23	25	26.5	26.5	26.5	26.5	26.5	25	23.5	21	18.5	16.5	14	9	6	4
$\times 10^4$	15	-25	-7	-10	-14	-17	-20	-21	-24	-26	-26.5	-26.5	-26.5	-26.5	-26.5	-25	-23	-21	-18	-16	-12	-9	-5	-2
Sum (c)	15	-25	-2	-15	-2	-2	-3	-2	-4	-1	0	0	0	0	0	0	.5	0	1.5	.5	2	2	3	2
Diff. (d)	-15	55	12	115	26	32	37	42	46	51	53	53	53	53	53	50	46.5	42	33.5	32.5	26	20	13	6

(c)	0	1	2	3	4	5	6	7	8	9	10	11		(d)	0	1	2	3	4	5	6	7	8	9	10	11
	12	23	24	34	44	19	18	17	16	15	14	13			11	33	22	21	20	19	18	17	16	15	14	13
	15	-2.5	-2	-1.5	-2	-2	-2	-2	-2	-1	0	0			-15	45	12	10.5	26	22	37	43	46	51	53	53
	0	2	2	2	2	.5	1.5	0	.5	0	0	0			53	7	13	16	26	35	37.5	43	46.5	50	53	53
Sum (e)	15	-.5	1	.5	0	-1.5	-1.5	-2	-1.5	-1	0	0		(g)	51.5	10.5	25	28.5	52	64.5	78.5	89	132.5	101	106	106
Diff. (f)	15	-4.5	-5	-3.5	-4	-2.5	-4.5	-2	-2.5	-1	0	0		(h)	-51.5	-4.5	-1	-1.5	0	-.5	-.5	0	-.5	1	0	0

	0	1	2	3	4	5									0	1	2	3	4	5				
(e)	6	11	10	9	8	7								(h)	6	11	10	9	8	7				
	15	-.5	1	.5	0	-1.5									-51.5	-4.5	-1	-1.5	0	-.5				
	-1.5	0	0	-1	-1.5	-2									-15	0	0	1	.5	0				
Sum (k)	0	-.5	1	-.5	-1.5	-2.5								Sum(m)	-55	-4.5	-1	-.5	-.5	-.5				
Diff. (l)	3	-.5	1	.5	1.5	.5								Diff.(n)	-51	-4.5	-1	-2.5	-.5	-.5				

(k)	0	1	2		(l)	0	1	2		(m)	0	1	2		(n)	0	1	2						
	9	8	4			3	5	4			3	5	4			3	5	4						
	0	-.5	1			3	-.5	1			-.55	-4.5	-1			-.51	-4.5	-1						
	-.5	-1.5	-1.5			1.5	.5	1.5			-.5	-.5	-.5			-2.5	-.5	-.5						
Sum (p)	-.5	-1	-.5		(r)	4.5	0	2.5		(t)	-55.5	-2	-1.5		(v)	-54.5	-2	-1.5						
Diff (q)	.5	3	.5		(s)	1.5	-1	-.5		(u)	-51.5	1	-.5		(w)	-52.5	-1	-.5						

$$\sqrt{3}\, M_{f_a}(\theta) = 2.6 \sin\omega t + .308 \sin(5\omega t) + [.209 \sin(2\omega t) + .0448 \sin(3\omega t) - .02 \sin 4\omega t]$$

APPENDIX II

DESIGN OF THE MAGNETIC MODULATOR

Power considerations on the prime mover Dumore motor, dictated the choice of a lower prf than was originally planned. It had been hoped that a prf of 10 kc could be attained, but it will be noticed that the no load rotational losses of the alternator are quite high. With a peak power of 15 kw at a prf of 5 kc, there is a duty ratio of 1/200 for a 1 microsecond pulse. This gives an average power of 75 watts. Assuming a modulator efficiency of 50% (10), this means that 150 watts of average power must be supplied from the alternator. At 5 kc the no load losses are approximately 190 watts as plotted in Fig. XII. Therefore this frequency was adopted for the full scale test, since it appeared to fall within the limitation of the ½ hp motor used to drive the alternator.

The Raytheon Package Magnetron, 2J38, was chosen since it was operative on low peak power of 15 kw. The operating point 4.95 kv at 3 amp. was selected, at 3260 mc. Thus the apparent magnetron resistance was fixed at 1.65 K.

APPENDIX II

DESIGN OF THE MAGNETIC AMPLIFIER

Power considerations on the prime mover Dynamo
motor, dictated the choice of a lower pitch than was originally
planned. It had been hoped that a pair of 10 kw could be
utilized, but it will be noticed that the no load rotational
losses of the alternator are quite high. With a peak power
of 15 kw at a pf of .5 lag, there is a duty ratio of 1/200
for a 1 microsecond pulse. This gives an average power of
75 watts. Assuming a modulator efficiency of 50% (10), while
assuming that 100 watts of average power must be supplied from
the alternator. At 5 kw the no load losses are approximately
190 watts as plotted in Fig. III. Therefore this frequency
was adopted for the full scale test, since it appeared to
fall within the limitation of the ½ hp motor used to drive
the alternator.

The Leyland Packard Engineering, 1939, was chosen
since it was operative on low peak power of 15 kw. The
operating point 1.05 kv at 5 amp. was selected, at 3250 rpm.
Then the apparent impedance was fixed at 1.05 Ω.

It would have been desirable to have obtained a pulse transformer with a turns ratio in the neighbourhood of 1:8, however, the maximum available was 1:5. Thus the resistance reflected across to the pulse forming network was $1.65 \times 10^3/5^2$ or 66 ohms. Since this value set the characteristic resistance of the artificial delay line and since the pulse duration was fixed at 1 microsecond arbitrarily, the parameters of the delay line were prescribed when the number of stages was set. This was fixed arbitrarily at five. With the number of stages set at five, the delay per stage for the PFN was fixed at 1/10th of a microsecond. Thus the two simultaneous equations were established:

$$\sqrt{LC} = .1 \times 10^{-6} \text{ seconds}$$

$$\sqrt{\frac{L}{C}} = 66 \text{ ohms}$$

$$C = .0015 \text{ microfarads}$$

$$L = 6.68 \text{ microhenries}$$

From Chapter II it is seen that C_o is specified now as 50 or .0075 microfarads. For resonance it is necessary that the formula be satisfied:

$$6.28 \times 5 \times 10^{3} = \frac{1}{\sqrt{L_t C_o}}$$

or $L_o + L_1 = 135$ millihenries

Note at this point that the internal inductance, L_1, of the alternator could be used to determine C_o for any value of frequency (prf). However, this would imply that the option is present to select any value of turns ratio in the pulse transformer, which option was not present in this investigation from practical considerations. L_o was therefore set at 135-8 = 127 mh.

The voltage relationships of the modulator are specified by the operating point picked for the magnetron. For a 5 kv peak pulse delivered to the magnetron, a 1 kv pulse is required from the artificial delay line. This specifies that the PFN must be charged to 2 kv prior to discharge and hence this in turn specifies the peak voltage to which C_o charges as 2 kv.

Now it is feasible to specify the turns to be placed on the cores. Both cores were of the same material but were manufactured by the Arnold Engineering Co. and Magnetics, Inc. respectively, hence the trade names Deltamax and Orthonol. This material can be compared on Fig. III

$$6.28 \times 5 \times 10^{-3} = \sqrt{\frac{R^2}{L^2}}$$

$$R^2 = 1.97 \text{ megohms}$$

Note at this point that the internal inductance, L^1, of the electrode could be used to determine C^0 for any value of temperature (part). However, this would imply that the medium is present to select any value of tube radio in the pulse transformer, which option was not present in this investigation from practical considerations. L^0 was therefore set at 130-0 = 127 mh.

The voltage relationship of the modulator are specified by the operating point plotted for the measurement. For a 5 kv peak pulse delivered to the magnetron, a 1 kv pulse is required from the artificial delay line. This specifies that the PFN must be charged to 2 kv prior to discharge and hence this in turn specifies the peak voltage to which C^0 charges as 2 kv.

How it is feasible to specify the turns to be placed on the cores. Both cores were of the same material but were manufactured by the Ferrolo Engineering Co. and Magnetics, Inc. respectively, hence the trade names Deltamax and Orthonol. This material can be compared on Fig. III

with other square loop materials; it will be seen that the flux density swing is large, the coercive force is low, the knees are sharp and the flatness of the manufacturer's saturation data indicates a low value of saturated permeability.

To compare dynamic performance, curves of Hysteresis were calculated, similar to that shown in Fig. XIII. From current-voltage relationships it was found that a change in frequency in the region of 5 kc showed no significant departure from a mean for that frequency. The loop for 3.12 kc is shown in the figure, for a #5387D1 core. The measured flux density swing was 24,500 gauss. The measured saturated permeability was 42 for this core. This was obtained by measuring the voltage across a saturated core, at 5 kc. The core, of course, was driven into saturation by a second auxiliary winding. Eight stacked matched Orthonol #50003 cores were used for the second saturable core. The measured flux density swing, $2\ B_m$, was 26,500 gauss with a saturated permeability of 12.

Both cores developed considerable heat in the switching process under test. Waveforms became distorted under current drive after more than ten minutes of operation and it was therefore deemed necessary to provide for operation of the cores under oil for cooling purposes.

with other square loop material it will be seen that the flux density swing is large, the coercive force is low, the losses are sharp and the flatness of the nonretentivity feature-tion data indicates a low value of retrieved permeability.

To compare dynamic performance, curves of hysteresis were obtained, similar to that shown in Fig. 5111. From current-voltage relationship it was found that a change in frequency in the region of 5 kc showed no significant departure from a mean for that frequency. The loop for 3.12 kc is shown in the figure, for a [illegible] core. The measured flux density swing was 2,300 gauss. The measured retentive permeability was 12 for this core. This was obtained by measuring the voltage across a saturated core, at 5 kc. The core, of course, was driven into saturation by a second positive pulsing. Eight standard matched [illegible] cores were used for the second saturable core. The measured flux density swing 2 B_m was 2,300 gauss with a retained permeability of 12.

Such cores developed considerable heat in the switching process under test. Investigations because disturbed under control duty also were done when minutes of operation and it was therefore deemed necessary to provide for operation of the cores under dit for cooling purposes.

For the main winding on the first stage core it was first necessary to determine the volt-time integral for 5 kc at a peak of 2 kv. This integral is given by the formula:

$$\int_0^{2\pi/\omega} e(t)\,dt = \frac{1.1\ E_{cop}}{\omega} \text{ v sec.}$$

Substituting into the formula:

$$N = \frac{\int e\,dt \times 10^8}{2B_m A}$$

$$= \frac{\frac{1.1 \times 2000}{2\pi \times 5000} \times 10^8}{24500 \times .404}$$

$$= 709 \text{ turns.}$$

For bias:

$$Hc\ \frac{NI}{l_m}$$

$$NI = H_c\ l_m = .39 \times 12 \text{ at}$$

= 4.7 net ampere turns desired for bias. (This value of bias on the first stage core will displace its B-H characteristic by an amount equal to the coercive force, which will enable use of full flux swing.)

$$(NI)_{av} = \frac{E_{cop}\, C_a}{T}$$

$$= \frac{200 \times .0075 \times 10^{-6} \times 709}{200 \times 10^{-6}}$$

= 53 ampere turns effective (due to the average current in SC1)

Therefore the amount of bias is determined by the difference required to return the curve to the desired coercive force; this is seen to be 53-4.7, say 48 ampere turns. For an arbitrary 50 turns on the bias winding, an amperage of -.96 amperes is required.

The volt-time integral of the voltage waveform across the PFN is obtained by integration of the analytical expression for this voltage, neglecting the second order effect of magnetizing current in the second stage core.

$$\int_0^{\pi\sqrt{L_{sc1_s}C'}} e_{pfn}(t)\, dt = \frac{E_{fnp}}{2} \int_0^{\pi\sqrt{L_{sc1_s}C'}} \left(1 - \cos \frac{1}{\sqrt{L_{sc1_s}C'}}\right) dt$$

$$\int_0^{\int_0^{\sec^2 C_1\, dx}} \frac{}{} \left(1+\frac{}{}\right) dx = \frac{}{} \int_0^{\sec^2 C_1\, dx}$$

$$\frac{E_{cop}\pi\sqrt{L_{scls}C'}}{2}$$

* Substituting values into this formula:

$$\frac{2000\,\pi\sqrt{8.9 \times .00375 \times 10^{-9}}}{2}$$

18.1×10^{-3} volt sec.

For the number of turns for the second stage core:

$$N = \frac{36.2 \times 10^{-3} \times 10^{8}}{26500 \times 8 \times .121}$$

$$= 70 \text{ turns}$$

(A is .121 cm^2 for one core)

The saturated inductance of the second stage core is computed to be:

$$L_{sc2s} = \frac{3.2\, N^2 \mu_3 A\ 10^{-8}}{l_m} \quad \text{(mixed English units)}$$

$$= \frac{3.2 \times 70^2 \times 8 \times .121 \times 10^{-8} \times 12}{2.54 \times 1.58}$$

$$= 17.8\ \mu h$$

$$*L_{ls} = 8.9 \text{ mh}$$

$$= \frac{7.5 \times 10^{5} \times 8 \times .121 \times 10^{-9} \times 13}{2.54 \times 1.59}$$

$$= 17.6 \text{ hy}$$

$$L_{2a} = 8.9 \text{ hy}$$

$$L_{2a(\text{desired})} = \frac{7.5 \times 10^{5} \times 8 \times .121 \times 10^{-8}}{1^{2}} \quad \text{(plane English units)}$$

The saturated inductance of the second stage core is computed to be:

$$L_{2a} = \frac{4\pi \times .121 \text{ in}^2 \text{ for one core})}{10 \text{ turns}}$$

$$= \frac{2500 \times 8 \times .121}{34.8 \times 10^{-3} \times 10^{8}}$$

For the number of turns for the second stage core:

$$10.1 \times 10^{-9} \text{ volt sec.}$$

Substituting values into this formula:

$$\frac{2000 \text{ volts} \times 0.5 \text{ } \mu\text{sec}}{\text{Delta B} \times .00754 \times 10^{-4}}$$

The last value should be satisfactory since it is of the estimated order of magnitude of stray inductance in the magnetron circuit.

The final computation in the design of the modulator is to check the damping constant of the charging circuit. The charging circuit consists of the internal resistance and armature inductance of the alternator, in series with the external inductance required for resonance and the charging capacitor, C_o.

The resistance necessary for critical damping is given by examination of the expression for the locations of the poles of the complex frequency response of the circuit.

$$s = \frac{-R}{2L} \pm \sqrt{\left(\frac{R}{2L}\right)^2 - \frac{1}{LC}}$$

where: R = internal resistance of the machine, R_1

L = total inductance of the charging circuit, $L_o + L_1$

C = charging capacitance, C_o

For critical damping the expression under the radical is zero and this occurs when:

$$\left(\frac{R}{2L}\right)^2 = \frac{1}{LC}$$

$$R = 2\sqrt{\frac{L}{C}}$$

[illegible]

[illegible]

[illegible]

For the values used in the modulator it is seen that this critical resistance is equal to:

$$R_c = 2\sqrt{\frac{135 \times 10^{-3}}{7.5 \times 10^{-9}}}$$

$$= 8500 \text{ ohms}$$

The ratio of this value of internal resistance to that required for critical damping is thus seen to be:

$$\frac{79}{8500} = .0093$$

From which calculation it is assumed that the damping effect is negligible. Therefore the waveform of the voltage across the charging capacitance should closely approximate the waveform of that obtained when damping is neglected completely, namely a waveform which charges to 3.14 x the excitation voltage, whose volt-time integral is given by 1.1 x 3.14 x the value of the excitation peak voltage.

For the values used in the calculation in the above

Case this critical resistance is equal to

$$R_c = 2\sqrt{\frac{1.25 \times 10^{-3}}{7.5 \times 10^{-6}}}$$

$$= 25.8 \text{ ohms}$$

The ratio of this value of internal resistance to that required for critical damping is thus seen to be:

$$\frac{25.8}{75} = .0081$$

Thus quick calculation is to be warned that the damping effect is negligible. Therefore the variations of the voltage across the charging capacitance should closely approximate the waveform of that obtained when damping is neglected completely, namely a waveform which changes to $1-1/e$ the excursion voltage, where exponential is given by $1-1 = 1-.63$ = the value of the excitation less voltage.

BIBLIOGRAPHY

1. "German Wartime Tchnical Developments", Transactions Soc. Naval Architects and Marine Engineers, Vol.54, 1946 pp 83-111, New York, N.Y.

2. "The Use of Saturable Reactors as Discharge Devices for Pulse Generators," Institution of Electrical Engineers Vol. 98, pps 185-204, London; Melville, W.S.

3. Magnetic Amplifiers NAVSHIPS 900,172, Navy Bureau of Ships, Washington 25, D.C.

4. Analysis of the Lubrication of Bearings, M.C. Shaw and E.F. Macks, McGraw Hill Book Co., New York, N.Y., 1949 pp 155-156

5. Analysis of the Lubrication of Bearings, M.C. Shaw and E.F. Macks, McGraw Hill Book Co., New Yrok, N.Y., 1949 pp 329-331

6. Analytical Mechanics for Engineers, F.B. Seeley and N.E. Ensign, John Wiley and Sons, New York, N.Y., 1941 pp 382-385.

7. Advanced Strength of Materials, J.P. Den Hartog, McGraw Hill Book Co., New York, 1952, pp 49-57

8. "Magnetic Core Pulse Amplifiers for Digital Computers" S.M. Thesis, M.I.T., Hawley K. Rising, 1953

9. "Production Testing of Tape Core Materials", J.E. Mitch, W.A. Lewis, R.A. Parnell, AIEE Conference Paper, June, 1954.

10. "An Investigation of Radar Magnetic Modulator Performance" Charles W. Simmonds, S.M. Thesis, M.I.T. August, 1954

BIBLIOGRAPHY

1. "Seismic Velocity Statistical Investigations", Proceedings
Conf. Appl. Statistics and Digital Computers, Calcutta, 1964,
pp 63-113, New York, N.Y.

2. "Time Use of Returning Travelers on Standard Service
for Video Conferences" Quantitation of Statistical Documents
Vol. 19, pps 345-369, Academic Society, U.S.

3. Computer Applications, Airports 000,212, Navy Bureau
of Medicine, Washington DC, U.S.

4. Analysis of the Fabrication of Bearings, R.T. Shaw and
S.T. Hanley, Academic Press Corp, New York, N.Y., 1962
pp 345-420

5. Analysis of the Fabrication of Bearings S.T. Shaw and
S.T. Hanley, Academic Press Corp, New York, N.Y., 1962
pp 345-420

6. Statistical Analysis for Geology, J.D. Hanley and
S.C. Hanley, Academic Press Corp, New York, N.Y., 1962
pp 389-392.

7. Aggregate Commerce of Computers, A.T. Van Hanley, Academic
Press Corp, New York, pps 63-67

8. "Aggregate Core Value Application for Digital Computers"
pp 45- Hanley, S.C.T., Academic Press Corp, 1963

9. "Precision Grading of Base Core Material", A.S. Hines,
A.A. Hanley, S.C., Journal, Air Conditioning Engr,
June, 1961.

10. "An Investigation of Solar Energie Insulator Performance"
Charles T. Hanover, U.S. Hanley, M.I.T. August, 1962

11. Principles of Radar , J.F. Reintjes and G.T. Coate McGraw Hill Book Co., New York, N.Y.

12. "The Theory of the Inductor Alternator" , J.H. Walker, Journal of the Institution of Electrical Engineers, Vol. 89, Part II, 1942; pp 227-241, London

13. "Theory of Pulsating Machines", R. Pohl, Journal of the Institution of Electrical Engineers , Vol. 93, Part II, 1946, PP37-47, London

14. "Open Circuit Characteristics of a High Frequency Inductor Alternator", P.W. Shelton, S.B. Thesis, MIT 1954.

15. "Design of a High Speed Inductor Alternator", J.T. Duane, S.M. Thesis, M.I.T., 1954

16. Radar System Engineering , Radiation Laboratory Series McGraw Hill Book Co, New York, N.Y., 1947

12. _Principles of Optics_, 6th ed. Pergamon Press and G.B. Tuttle Bookcraft Ltd. Salt Lake City, U.S.A.

13. "The Theory of the Achromatic Microscope", J.H. Wilson, _Journal of the Institute of Electrical Engineers_, Vol. 17, Part II, 1948, pp. 217-224, London.

14. "Theory of Reducing Reactions", H. Veil, _Journal of the Institution of Electrical Engineers_, Vol. 17, Part II, 1948, pp. 217-224, London.

15. "Some Cosmic Correspondence of a High Dependency Behavior Criterion", Pro. Meeting, U.S. Rubber, pp. 1948.

16. "Theory of a High Speed Tabulator Alternator", U.S. Patent, 8,8, 1948.

17. _Basic Servo Engineering_, Bartholin Laboratory Series Series #13 Wiley Co, New York, U.S.A. 1947

Thesis
R667 Rodgers
Radar magnetic modulation using a high frequency induction alternator power source.
28782

Thesis
R667 Rodgers
Radar magnetic modulation using a high frequency induction alternator power source.
28782

thesR667
Radar magnetic modulation using a high f
3 2768 001 94937 3
DUDLEY KNOX LIBRARY